



City Research Online

City, University of London Institutional Repository

Citation: Papkov, S. O. & Banerjee, J. R. (2022). Dynamic stiffness formulation for isotropic and orthotropic plates with point nodes. *Computers & Structures*, 270, 106827. doi: 10.1016/j.compstruc.2022.106827

This is the published version of the paper.

This version of the publication may differ from the final published version.

Permanent repository link: <https://openaccess.city.ac.uk/id/eprint/28354/>

Link to published version: <https://doi.org/10.1016/j.compstruc.2022.106827>

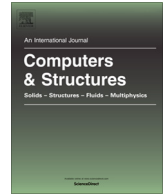
Copyright: City Research Online aims to make research outputs of City, University of London available to a wider audience. Copyright and Moral Rights remain with the author(s) and/or copyright holders. URLs from City Research Online may be freely distributed and linked to.

Reuse: Copies of full items can be used for personal research or study, educational, or not-for-profit purposes without prior permission or charge. Provided that the authors, title and full bibliographic details are credited, a hyperlink and/or URL is given for the original metadata page and the content is not changed in any way.

City Research Online:

<http://openaccess.city.ac.uk/>

publications@city.ac.uk



Dynamic stiffness formulation for isotropic and orthotropic plates with point nodes

S.O. Papkov^a, J.R. Banerjee^{b,*}

^a Department of Mathematics, Sevastopol State University, Sevastopol, Crimea, Russia

^b School of Mathematics, Computer Science and Engineering, City, University of London, United Kingdom

ARTICLE INFO

Article history:

Received 14 February 2022

Accepted 14 May 2022

Keywords:

Orthotropic plate

Free vibration

Natural modes

Dynamic stiffness matrix

Discrete Fourier transform

ABSTRACT

In this paper, the dynamic stiffness method for isotropic and orthotropic rectangular plates with point nodes is developed, making it possible to integrate the dynamic stiffness properties for plates with the dynamic stiffness properties of other elements such as bars and beams, but importantly, the advanced theory allows amalgamation of the dynamic stiffness method with the conventional finite element method for the first time. The derivation of the dynamic stiffness matrices for isotropic and orthotropic plates with point nodes has been accomplished by implementing the Fourier coefficients of the boundary values of the amplitudes of forces and displacements of the plate to form the force–displacement relationship at nodal points, including the corners. This innovative objective has been achieved by developing a new form of discrete Fourier transform technique for modified trigonometric functions. Using some carefully chosen illustrative examples, the convergence of results is ascertained by using different number of node points and their locations on the plate edges. The proposed theory has substantial advantages over conventional dynamic stiffness theories for plates, particularly when applying non-classical different boundary conditions on plate edges. The computed numerical results are discussed with significant conclusions drawn.

© 2022 The Authors. Published by Elsevier Ltd. This is an open access article under the CC BY license (<http://creativecommons.org/licenses/by/4.0/>).

1. Introduction

For free vibration analysis of structures, the dynamic stiffness method (DSM) is well-known as a powerful alternative to the finite element method (FEM) with significantly better model accuracy. This is mainly because DSM is a differential equation model whereas FEM is based on assumed shape functions. In the early seventies, Wittrick and Williams developed the DSM for isotropic and anisotropic rectangular plates when two opposite sides of the plate are simply supported [1]. Side by side to this work, they also developed a robust solution technique [2,3] for the DSM to extract the eigenvalues of the structure, which are generally natural frequencies in free vibration problem and critical load factors in buckling problem. Their solution technique [2,3] was really a breakthrough and it is now known as the Wittrick-Williams algorithm which has featured in literally hundreds of papers. The DSM is an exact method which uses exact solution of the governing differential equations of the boundary value problem of a freely vibrating structure. Prior to the development of the DSM, the transverse vibration problem of an individual rectangular plate with

two opposite edges simply supported was solved in an exact sense by many investigators using the so-called Levy type solution [4–6]. This is relatively an easy task because the mode shapes in one of the directions are sine functions for the simply supported plate, which made the governing bi-harmonic equation of the plate amenable to exact solution. These investigations are by and large, mostly confined to single plates rather than an assembly of plates, but of course approximate solution for plates and plate assemblies using different boundary conditions can be successfully obtained by using the FEM [7–8]. Levy type solution for simply supported plates has been suitably extended to cover anisotropic plates [9] and there are also some refined plate theories in the published literature [10–12]. Clearly, for the case of a simply supported plate, there exists an exact solution for the free transverse vibration in the form of a trigonometric series whereas for other boundary conditions, there are approximate methods such as Rayleigh-Ritz [13–15], extended Kantorovich [16], Galerkin [17,18], differential quadrature [19] and boundary element [20,21] amongst a few other methods. Using the Levy type solution one can build an accurate, if not exact, analytical relationship between the amplitudes of forces and displacements at the plate boundaries which are basically the sides or edges of the plate. The relationship essentially defines the dynamic stiffness matrix of a simply supported plate

* Corresponding author.

E-mail address: j.r.banerjee@city.ac.uk (J.R. Banerjee).

element as originally reported by Wittrick and Williams [1]. Following the work of Wittrick and Williams, Boscolo and Banerjee [22,23] applied DSM and improved the quality of the dynamic stiffness element for plates by including the first order shear deformation theory. Pagani et al. [24] developed DSM for multi-layered structures by using higher order theories to investigate their free vibration characteristics. Other notable contributors are, amongst others, Eisenberger and Deutsch [25], Casimir et al. [26] and Ghorbel et al. [27] who used DSM to solve the plate vibration problem. The application of DSM to shell structure is outside the scope of this paper, but interested readers are referred to the work of Fazzolari [28] and Chen and Ye [29].

It should be noted at this point that by assembling the dynamic stiffness matrices of individual elements in a structure, it is possible to construct the global dynamic stiffness matrix of the final structure and then the natural frequencies of the final structure can be computed in a straightforward manner by applying the Wittrick-Williams algorithm [2]. In this way, complex structures can be analyzed for their free vibration characteristics by using the DSM. There are established computer programs [30,31] to accomplish such tasks. The area of applicability of DSM for plates was significantly narrowed in the past by the assumption of Levy type solution, based on the premises that the two opposite sides of the plate are simply supported. Overcoming this restriction continued to be a daunting task for many years. The difficulty was primarily associated with seeking an exact general solution for the bi-harmonic equation which governs the free vibration behaviour of a plate for the most general case. The much-expected breakthrough for the DSM development of plates for the general case, came in recent years when the DSM approach for free vibration analysis of rectangular plates and their assemblies with any arbitrary boundary conditions became an area of intense research activity, see for example Nefovska-Danilovich et al. [32,33] and Kim and Lee [34]. Some background information is necessary to explain how the limitation of the classical DSM based on simply supported boundary conditions of rectangular plates was overcome. Gorman's superposition method [35–37] although different from DSM, was a significant development which stimulated the research in the advancement of DSM for general boundary conditions of plates. By using Gorman's superposition method [35–37], the infinite series representing the general solution of the plate can be truncated at some suitable point to achieve reasonable accuracy. However, for the computation of higher order natural frequencies, it would be necessary to increase the number of terms needed in the series which cannot be predicted easily in advance. To alleviate this problem, Banerjee et al. [38] developed DSM for a rectangular plate with any arbitrary boundary conditions by taking full advantage of the symmetry of the plate, but importantly by considering the effect of the remainders of the infinite series solution beyond the cut-off point. This was ignored by other investigators. (In this context, it is worth noting that Papkov [39] demonstrated the importance of considering the remainders of the infinite series terms in free vibration analysis, which have significant effect on the accuracy of results.) Essentially, the authors of [38] split the plate into four equal quarters and then on the enforced planes of symmetry, they applied all four possible boundary conditions which are: (i) symmetric-symmetric (SS), (ii) symmetric-anti-symmetric (SA), (iii) anti-symmetric-symmetric (AS) and (iv) anti-symmetric-anti-symmetric (AA). In this way, they constructed the dynamic stiffness matrix of each of the four components in an exact sense and the overall dynamic stiffness matrix was obtained by summing up the individual dynamic stiffness matrices for all four cases. The symmetry reduced the size of the problem, and there was no approximation involved in the theory in any way. In their formulation, Banerjee et al. [38] used an exact inversion of an infinite matrix system based on an asymptotic expansion of

linear equations to derive the dynamic stiffness matrix. This is in sharp contrast to the work described in [32,33]. One of the main differences between [38] and [32,33] is that the former publication accounts for the infinite remainders of the series solution of the plate whereas the latter publications do not make allowances of the remaining terms of the infinite series by truncating it. In this respect, a recently published paper by Kim and Lee [34] makes interesting reading. Although the notations used in [34] are different from [38], nevertheless, the authors of [34] applied quite a similar approach to that of [38], but there were some significant differences too. The solution in [34] was described as a sum of two partial solutions unlike [38] where the solution was not split in that way. One of the other differences was that [34] used exponential Fourier series representation in the solution which contrasts with trigonometric form of solution in [38]. Liu and Banerjee [40] generalized the approach presented in [38] when they investigated the free vibration behaviour of orthotropic plates. Recently, Wei et al [41] made a noteworthy contribution when they formulated the dynamic stiffness matrix for transverse and in-plane vibration of rectangular plates with arbitrary boundary conditions. Their work differs from the work described in [38,42,43] in that the choice of the trigonometric function to describe the series solution was somehow different, which yielded slightly different results. It should be noted that strictly speaking, for all the above approaches, the dynamic stiffness matrix in the exact formulation is an infinite matrix because the boundary values of the displacements and forces form an infinite system of equations. All the above publications dealt with dynamic stiffness formulation for plates with line nodes and none of the previous publications dealt with the dynamic stiffness formulation for plates with point nodes. Regarding this matter, the following comments are made.

The assumed shape functions utilized in FEM are generally lower order polynomials, and thus the formulation of the free vibration problem somehow leads to acceptably good results, particularly in the low and medium frequency ranges, but in the high frequency range, the results from FEM become progressively less accurate. Attempts to improve results using FEM have been made by some investigators by using higher order polynomials which enhance the shape function representation of the structural deformation, see for example Kulla [44]. On the other hand, Doyle [45], and Lee [46] developed spectral element method (SEM) using frequency-dependent trigonometric and hyperbolic functions to address the free vibration problem of plates. Interestingly, Birgersson et al [47] went a step further and proposed a spectral super element model in their endeavour to improve the accuracy of results for the plate vibration problem. In many ways, SEM is similar to DSM as it does not construct separate element mass and stiffness matrices, unlike the FEM. Thus, SEM is effectively a spectral version of the DSM and basically, the two methods differ mainly in their numerical implementation when obtaining results.

Despite significant progress made over the years, the DSM has not still been established as a sufficiently versatile tool like the FEM, even though DSM is properly recognized as a powerful and accurate alternative to FEM, but admittedly DSM is used to solve a specific minority group of vibration problems. Without an effective integration of DSM with FEM which has much greater distribution and coverage, the application of DSM, particularly for plate elements remains strictly restricted. For two-noded line elements such as bars and beams, the task of combining DSM and FEM is relatively simple and straightforward [48], but for plate elements, the problem is extremely difficult. This is mainly because the DSM research for plate elements so far has continued to use line nodes whereas the FEM understandably works very well with point nodes for structural elements. The dynamic stiffness formulation for plate elements relating boundary forces with boundary dis-

placements at some chosen nodal points will no-doubt be a significant step forward which can be exploited to great advantage with possible amalgamation of DSM with FEM. If the versatility of FEM is combined with the uncompromising accuracy of DSM, the scope of structural analysis with hybrid computational algorithm will no-doubt be substantially enhanced. Thus, the essential purpose of this paper is to develop through the applications of the exact solution of the governing differential equation, the dynamic stiffness matrix for isotropic and orthotropic plates characterized by nodal points. The resulting dynamic stiffness matrix with point nodes developed in this paper is finally applied through the implementation of the Wittrick-William algorithm as solution technique to compute natural frequencies and mode shapes for a wide range of problems and some of the results are validated against published results. The accuracy of results on the choice of the number of selective nodes on the plate edges is also demonstrated. The paper concludes with its principal findings with the expectation that it will pave the way for further research in DSM.

2. Dynamic stiffness formulation for a plate with line nodes

The investigation is aimed to show in an ingenious way, how the dynamic stiffness matrix of a plate with line nodes can be transformed into its dynamic stiffness matrix with point nodes. The line-nodes to point-nodes transformation can be carried out either partly or fully, depending on the nature of the problem. Clearly, the important step to generate the dynamic stiffness matrix of a plate with point nodes cannot be fruitfully accomplished unless the preliminary step of generating its dynamic stiffness matrix with line nodes is successfully completed. This useful extension from line nodes to point nodes, being far from trivial, is of considerable complexity and some preludes are required to lead the reader smoothly into the subject matter. Let us consider a uniform rectangular plate made of either isotropic or orthotropic material with sides $2a$ and $2b$, thickness h , and density ρ , as shown in a right-handed rectangular Cartesian coordinate system in Fig. 1. Within the framework of the classical Kirchhoff-Love hypothesis, the governing differential equation of motion of the plate in free bending vibration with the usual assumption of harmonic oscillation is given by

$$D_1 \frac{\partial^4 W}{\partial x^4} + 2D_3 \frac{\partial^4 W}{\partial x^2 \partial y^2} + D_2 \frac{\partial^4 W}{\partial y^4} - \lambda^4 W = 0 \quad (1)$$

where W is the amplitude of the bending displacement w^0 of the mid-plane of the plate so that the assumption of harmonic oscillation $w^0(x, y, t) = W(x, y)e^{i\omega t}$ is satisfied.

In Eq. (1), the terms D_1 , D_2 , D_3 and the frequency parameter λ are given by.

$$\begin{aligned} D_1 &= \frac{E_1 h^3}{12(1 - \nu_{12}\nu_{21})}; D_2 = \frac{E_2 h^3}{12(1 - \nu_{12}\nu_{21})}; \\ D_3 &= \frac{\nu_{12}E_2 h^3}{12(1 - \nu_{12}\nu_{21})} + \frac{G_{12} h^3}{6}; \lambda^4 = \omega^2 \rho h \end{aligned} \quad (2)$$

where E_1 , E_2 , G_{12} and ν_{12} (or ν_{21}) are the usual elastic constants for the orthotropic plate.

For isotropic plates

$$D_1 = D_2 = D_3 = D = \frac{Eh^3}{12(1 - \nu^2)} \quad (3)$$

with

$$E_1 = E_2 = E; \nu_{12} = \nu_{21} = \nu; G_{12} = G = \frac{E}{2(1 + \nu)} \quad (4)$$

To make the computed results from the new theory sufficiently general, particularly when covering plates and plate assembly with different geometries and different materials, we introduce a non-dimensional frequency parameter Ω which is related to the (dimensional) frequency parameter λ as follows

$$\Omega^4 = \frac{L^4 \lambda^4 \rho_0}{\rho D} \quad (5)$$

where D is the average flexural stiffness, ρ_0 is the average mass density when considering all plates in the structure and L is the half of the length of the structure (for a single plate $L = a$). The parameters D and ρ_0 are:

$$D = \sum_l \frac{S_l}{S} D_l; \quad (6)$$

$$\rho_0 = \sum_l \frac{S_l}{S} \rho_l \quad (7)$$

where S_l , D_l and ρ_l are area, flexural rigidity, and density of material of the l -th plate in the structure; S is the full surface area of the complete structure. The usefulness of this non-dimensionalisation leading to

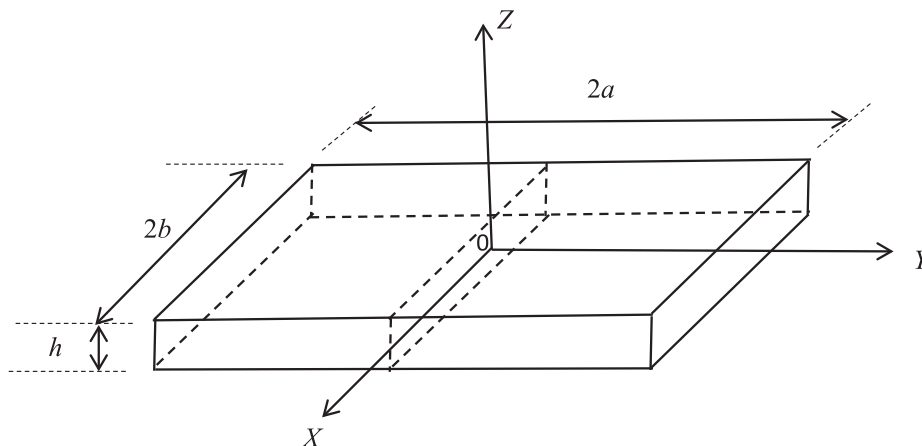


Fig. 1. Coordinate system and notation for a rectangular plate.

the parameter Ω will become apparent when analysing assembly of dissimilar isotropic or orthotropic plates with different properties.

To construct the dynamic stiffness matrix of the plate shown in Fig. 1, we introduce the following vectors for the amplitudes of boundary displacements and boundary forces

$$d = \begin{bmatrix} W_1 \\ \phi_1 \\ W_2 \\ \phi_2 \\ W_3 \\ \phi_3 \\ W_4 \\ \phi_4 \end{bmatrix} = \begin{bmatrix} W(a, y) \\ \phi_y(a, y) \\ W(x, b) \\ \phi_x(x, b) \\ W(-a, y) \\ \phi_y(-a, y) \\ W(x, -b) \\ \phi_x(x, -b) \end{bmatrix}; \quad f = \begin{bmatrix} V_1 \\ M_1 \\ V_2 \\ M_2 \\ V_3 \\ M_3 \\ V_4 \\ M_4 \end{bmatrix} = \begin{bmatrix} V_x(a, y) \\ M_x(a, y) \\ V_y(x, b) \\ M_y(x, b) \\ V_x(-a, y) \\ M_x(-a, y) \\ V_y(x, -b) \\ M_y(x, -b) \end{bmatrix} \quad (8)$$

We further introduce the following expressions based on the expansions of the trigonometric functions denoted by T_k .

$$d = \begin{bmatrix} W_a^+ \\ \phi_a^+ \\ W_b^+ \\ \phi_b^+ \\ W_a^- \\ \phi_a^- \\ W_b^- \\ \phi_b^- \end{bmatrix} = \sum_{k=0}^1 \sum_{n=1}^{\infty} \begin{bmatrix} W_{an}^{+k} T_k(\beta_{nk} y) \\ \phi_{an}^{+k} T_k(\beta_{nk} y) \\ W_{bn}^{+k} T_k(\alpha_{nk} x) \\ \phi_{bn}^{+k} T_k(\alpha_{nk} x) \\ W_{an}^{-k} T_k(\beta_{nk} y) \\ \phi_{an}^{-k} T_k(\beta_{nk} y) \\ W_{bn}^{-k} T_k(\alpha_{nk} x) \\ \phi_{bn}^{-k} T_k(\alpha_{nk} x) \end{bmatrix};$$

$$f = \begin{bmatrix} V_a^+ \\ M_a^+ \\ V_b^+ \\ M_b^+ \\ V_a^- \\ M_a^- \\ V_b^- \\ M_b^- \end{bmatrix} = \sum_{k=0}^1 \sum_{n=1}^{\infty} \begin{bmatrix} V_{an}^{+k} T_k(\beta_{nk} y) \\ M_{an}^{+k} T_k(\beta_{nk} y) \\ V_{bn}^{+k} T_k(\alpha_{nk} x) \\ M_{bn}^{+k} T_k(\alpha_{nk} x) \\ V_{an}^{-k} T_k(\beta_{nk} y) \\ M_{an}^{-k} T_k(\beta_{nk} y) \\ V_{bn}^{-k} T_k(\alpha_{nk} x) \\ M_{bn}^{-k} T_k(\alpha_{nk} x) \end{bmatrix} \quad (9)$$

where the trigonometric functions T_k depending on the type of symmetry are represented by

$$T_k(z) = \cos\left(\frac{\pi k}{2} - z\right) = \begin{cases} \cos z, & k = 0 \\ \sin z, & k = 1 \end{cases} \quad (10)$$

The separation constants α_{nk} and β_{nk} in Eq. (9) are chosen to be of the following form

$$\alpha_{nk} = \frac{\pi}{a} \left(n - 1 + \frac{k}{2}\right); \quad \beta_{nk} = \frac{\pi}{b} \left(n - 1 + \frac{k}{2}\right) \quad (11)$$

It should be noted that the chosen form of the trigonometric functions in Eqs. (9)-(11) are complete in their entirety to represent any type of boundary conditions for displacements and forces on the enforced planes of symmetry on the edges of the quarter plate, i.e., on the XZ and YZ planes of symmetry in Fig. 1.

By its definition, the dynamic stiffness matrix of a structural element characterizes the relationship between the boundary values of the amplitudes of forces and the corresponding displacements of the element when it is subjected to free natural vibration. The boundaries could be nodal points or nodal lines. For a rectangular plate with two opposite edges simply supported [1,22,23], this dependency for line nodes, can be analytically obtained for each vibration mode separately, say for the n -th mode, it is given by

$$f_{sn} = K_n \cdot d_{sn} \quad (12)$$

where

$$d_{sn} = \left(\begin{array}{l} W_{an}^{+0}, W_{an}^{+1}, \phi_{an}^{+0}, \phi_{an}^{+1}, W_{bn}^{+0}, W_{bn}^{+1}, \phi_{bn}^{+0}, \phi_{bn}^{+1}, W_{an}^{-0}, \\ W_{an}^{-1}, \phi_{an}^{-0}, \phi_{an}^{-1}, W_{bn}^{-0}, W_{bn}^{-1}, \phi_{bn}^{-0}, \phi_{bn}^{-1} \\ V_{an}^{+0}, V_{an}^{+1}, M_{an}^{+0}, M_{an}^{+1}, V_{bn}^{+0}, V_{bn}^{+1}, M_{bn}^{+0}, M_{bn}^{+1}, V_{an}^{-0}, V_{an}^{-1}, \\ M_{an}^{-0}, M_{an}^{-1}, V_{bn}^{-0}, V_{bn}^{-1}, M_{bn}^{-0}, M_{bn}^{-1} \end{array} \right) \quad (13)$$

$n = 0, 1, 2, \dots$

and K_n is the dynamic stiffness matrix of the plate for the n th mode. with the superscripts +0 for even components of boundary values when $x = a$ or $y = b$;

+1 for odd components of boundary values when $x = a$ or $y = b$;
- 0 for even components of boundary values when $x = -a$ and $y = -b$;

- 1 for odd components of boundary values when $x = -a$ and $y = -b$;

and the subscript n represents the number of Fourier coefficient for the n -th mode.

This dynamic stiffness matrix for a rectangular plate can be derived by using the following three steps:

- (i) Seek a general solution of the governing differential equation of the plate, i.e., Eq. (1) with enough number of undefined constants to satisfy any prescribed arbitrary boundary conditions on the plate edges. (In a Levy type plate for which the two opposite sides of the plate are simply supported, an exact solution is of course, possible.)
- (ii) For the general case, the solution is expanded in the form of trigonometric series to cover all possible boundary displacements and boundary forces.
- (iii) By imposing the boundary conditions, the undefined constants appearing in the general solution are eliminated for each vibrational mode with number n , which eventually gives the individual block of dynamic stiffness matrix K_n for the n -th mode.

The above procedure will be followed for any arbitrary boundary conditions of the plate all round its edges, but with the important difference here is that the solution will no longer be split into separate modes. The representation of the boundary expressions in Eq. (9) defines the form of the general solution of the governing differential equation given by Eq. (1). The composition of the solution is based on the separation of variables technique for each of the four component cases of symmetry [38,42] which are described above by symmetric-symmetric (SS), symmetric-anti-symmetric (SA), anti-symmetric-symmetric (AS) and anti-symmetric-anti-symmetric (AA), respectively. The complete general solution for the amplitude of the bending displacement W is given by the sum of all the four individual comments of the symmetry as follows

$$W = W_{00} + W_{01} + W_{10} + W_{11} \quad (14)$$

where the subscripts 0 and 1 on W on the right-hand side represent symmetry (S) and anti-symmetry (A) about the X and Y axes, respectively with 0 meaning symmetry and 1 meaning anti-symmetry. For example, W_{00} represents the solution for the case when the quarter plate in Fig. 1 is symmetric about both X and Y axes (SS) whereas W_{01} represents the solution corresponding to symmetry about the X axis and anti-symmetry about the Y axis (SA) and so on [38].

Referring to Fig. 1, the bending rotations ϕ_x and ϕ_y of the plate cross-section about the X and Y axes, the bending moments M_x and

M_y and shear forces V_x and V_y can be expressed in the usual notation as

$$\phi_x = \frac{\partial W}{\partial y}; \quad \phi_y = \frac{\partial W}{\partial x}; \quad (15)$$

$$V_x = - \left(D_1 \frac{\partial^3 W}{\partial x^3} + (D_3 + 2D_{66}) \frac{\partial^3 W}{\partial x \partial y^2} \right);$$

$$V_y = - \left(D_2 \frac{\partial^3 W}{\partial y^3} + (D_3 + 2D_{66}) \frac{\partial^3 W}{\partial x^2 \partial y} \right); \quad (16)$$

$$M_x = - \left(D_1 \frac{\partial^2 W}{\partial x^2} + D_{12} \frac{\partial^2 W}{\partial y^2} \right); \quad M_y = - \left(D_2 \frac{\partial^2 W}{\partial y^2} + D_{12} \frac{\partial^2 W}{\partial x^2} \right); \quad (17)$$

where $D_{12} = \nu_{12}D_2 = \nu_{21}D_1$ and $D_{66} = G_{12}h^3/12$ and D_1, D_2 and D_3 have already been defined earlier (see Eqs. (2) and (3)).

Following similar procedure as in [38,42] it is now possible to write the general solution of Eq. (1) in the form of infinite series for all four cases of symmetry as

$$W_{kj} = \sum_{n=1}^{\infty} (A_n H_j(p_{nk}y) + B_n H_j(\bar{p}_{nk}y)) T_k(\alpha_{nk}x) + \sum_{n=1}^{\infty} (C_n H_k(q_{nj}x) + D_n H_k(\bar{q}_{nj}x)) T_j(\beta_{nj}y) \quad (18)$$

The choice of hyperbolic function $H_k(z)$ in Eq. (18) depends on the type of symmetry and in particular,

$$H_0(z) = \cosh(z); \quad H_1(z) = \sinh(z) \quad (19)$$

Each term in the general solution of Eq. (18) satisfies exactly the governing differential Eq. (1) when the values p_{nk}, \bar{p}_{nk} and q_{nj}, \bar{q}_{nj} are the roots of the following characteristic equations

$$D_2 p^4 - 2D_3 \alpha^2 p^2 + D_1 \alpha^4 - \frac{D \rho_0}{\rho L^4} \Omega^4 = 0 \quad (20)$$

$$D_1 q^4 - 2D_3 \beta^2 q^2 + D_2 \beta^4 - \frac{D \rho_0}{\rho L^4} \Omega^4 = 0 \quad (21)$$

It has been shown earlier by Banerjee et al. [38], that the analysis of each case of symmetry is a separate problem on its own which makes it necessary to account for the terms corresponding to the constant components of the trigonometric expansions for each case, separately. The proposed form of Eq. (18) leads to create different, but analogous expressions for the solution of each of the four cases of symmetry which can be combined later to obtain the general solution.

Now the bending rotations of the plate cross-section about X and Y axes can be derived with help of Eqs. (15) and (18) to give

$$\phi_y = \sum_{n=1}^{\infty} (A_n^{kj} H_j(p_{nk}y) + B_n^{kj} H_j(\bar{p}_{nk}y)) \alpha_{nk} T'_k(\alpha_{nk}x) + \sum_{n=1}^{\infty} (C_n^{kj} q_{nj} H'_k(q_{nj}x) + D_n^{kj} \bar{q}_{nj} H'_k(\bar{q}_{nj}x)) T_j(\beta_{nj}y) \quad (22)$$

$$\phi_x = \sum_{n=1}^{\infty} (A_n^{kj} p_{nk} H'_j(p_{nk}y) + B_n^{kj} \bar{p}_{nk} H'_j(\bar{p}_{nk}y)) T_k(\alpha_{nk}x) + \sum_{n=1}^{\infty} (C_n^{kj} H_k(q_{nj}x) + D_n^{kj} H_k(\bar{q}_{nj}x)) \beta_{nj} T'_j(\beta_{nj}y) \quad (23)$$

With the help of Eqs. (16) and (18), the expressions for shear forces can be obtained as.

$$V_x = \sum_{n=1}^{\infty} (A_n^{kj} [D_1 \alpha_{nk}^2 - (D_3 + 2D_{66}) p_{nk}^2] H_j(p_{nk}y) + B_n^{kj} [D_1 \alpha_{nk}^2 - (D_3 + 2D_{66}) \bar{p}_{nk}^2] H_j(\bar{p}_{nk}y)) \alpha_{nk} T'_k(\alpha_{nk}x) + \sum_{n=1}^{\infty} (C_n^{kj} q_{nj} [(D_3 + 2D_{66}) \beta_{nj}^2 - D_1 q_{nj}^2] H'_k(q_{nj}x) + D_n^{kj} \bar{q}_{nj} [(D_3 + 2D_{66}) \beta_{nj}^2 - D_1 \bar{q}_{nj}^2] H'_k(\bar{q}_{nj}x)) T_j(\beta_{nj}y) \quad (24)$$

$$V_y = \sum_{n=1}^{\infty} (A_n^{kj} p_{nk} [(D_3 + 2D_{66}) \alpha_{nk}^2 - D_2 p_{nk}^2] H'_j(p_{nk}y) + B_n^{kj} \bar{p}_{nk} [(D_3 + 2D_{66}) \alpha_{nk}^2 - D_2 \bar{p}_{nk}^2] H'_j(\bar{p}_{nk}y)) T_k(\alpha_{nk}x) + \sum_{n=1}^{\infty} (C_n^{kj} [D_2 \beta_{nj}^2 - (D_3 + 2D_{66}) q_{nj}^2] H_k(q_{nj}x) + D_n^{kj} [D_2 \beta_{nj}^2 - (D_3 + 2D_{66}) \bar{q}_{nj}^2] H_k(\bar{q}_{nj}x)) \beta_{nj} T'_j(\beta_{nj}y) \quad (25)$$

Next, we can express the undefined coefficients C_n^{kj} and D_n^{kj} for each case of symmetry (k, j) by means of the expansions of the coefficients of the boundary values of bending rotation $\phi_y(\pm a, y)$ and shear force $V_x(\pm a, y)$ in the first instance. By making use of Eqs. (22)–(25) and imposing the boundary conditions in Eq. (9) give the following system for Fourier coefficients

$$\sum_{k=0}^1 (C_n^{kj} q_{nj} H'_k(q_{nj}a) + D_n^{kj} \bar{q}_{nj} H'_k(\bar{q}_{nj}a)) = \phi_{an}^{+j} \quad (26)$$

$$\sum_{k=0}^1 (-1)^{k+1} (C_n^{kj} q_{nj} H'_k(q_{nj}a) + D_n^{kj} \bar{q}_{nj} H'_k(\bar{q}_{nj}a)) = \phi_{an}^{-j} \quad (27)$$

$$\sum_{k=0}^1 (C_n^{kj} q_{nj} [(D_3 + 2D_{66}) \beta_{nj}^2 - D_1 q_{nj}^2] H'_k(q_{nj}a) + D_n^{kj} \bar{q}_{nj} [(D_3 + 2D_{66}) \beta_{nj}^2 - D_1 \bar{q}_{nj}^2] H'_k(\bar{q}_{nj}a)) = V_{an}^{+j} \quad (28)$$

$$\sum_{k=0}^1 (-1)^{k+1} (C_n^{kj} q_{nj} [(D_3 + 2D_{66}) \beta_{nj}^2 - D_1 q_{nj}^2] H'_k(q_{nj}a) + D_n^{kj} \bar{q}_{nj} [(D_3 + 2D_{66}) \beta_{nj}^2 - D_1 \bar{q}_{nj}^2] H'_k(\bar{q}_{nj}a)) = V_{an}^{-j} \quad (29)$$

The subtraction and addition of Eqs. (26) and (27) give

$$\left. \begin{aligned} C_n^{0j} q_{nj} H'_0(q_{nj}a) + D_n^{0j} \bar{q}_{nj} H'_0(\bar{q}_{nj}a) &= \frac{\phi_{an}^{+j} - \phi_{an}^{-j}}{2} \\ C_n^{1j} q_{nj} H'_1(q_{nj}a) + D_n^{1j} \bar{q}_{nj} H'_1(\bar{q}_{nj}a) &= \frac{\phi_{an}^{+j} + \phi_{an}^{-j}}{2} \end{aligned} \right\} \quad (30)$$

Similarly, the subtraction and addition of Eqs. (28) and (29) give

$$\left. \begin{aligned} C_n^{0j} q_{nj} [(D_3 + 2D_{66}) \beta_{nj}^2 - D_1 q_{nj}^2] H'_0(q_{nj}a) + D_n^{0j} \bar{q}_{nj} [(D_3 + 2D_{66}) \beta_{nj}^2 - D_1 \bar{q}_{nj}^2] H'_0(\bar{q}_{nj}a) &= \frac{V_{an}^{+j} - V_{an}^{-j}}{2} \\ C_n^{1j} q_{nj} [(D_3 + 2D_{66}) \beta_{nj}^2 - D_1 q_{nj}^2] H'_1(q_{nj}a) + D_n^{1j} \bar{q}_{nj} [(D_3 + 2D_{66}) \beta_{nj}^2 - D_1 \bar{q}_{nj}^2] H'_1(\bar{q}_{nj}a) &= \frac{V_{an}^{+j} + V_{an}^{-j}}{2} \end{aligned} \right\} \quad (31)$$

The system of four equations for the undefined constants C_n^{kj} and D_n^{kj} given by Eqs. (30) and (31) can now be expressed as

$$\left. \begin{aligned} C_n^{kj} q_{nj} H'_k(q_{nj}a) &= \frac{D_1 \bar{q}_{nj}^2 - (D_3 + 2D_{66}) \beta_{nj}^2}{D_1 (\bar{q}_{nj}^2 - q_{nj}^2)} \cdot \frac{\phi_{an}^{+j} - (-1)^k \phi_{an}^{-j}}{2} + \frac{1}{D_1 (\bar{q}_{nj}^2 - q_{nj}^2)} \cdot \frac{V_{an}^{+j} - (-1)^k V_{an}^{-j}}{2} \\ D_n^{kj} \bar{q}_{nj} H'_k(\bar{q}_{nj}a) &= - \frac{D_1 q_{nj}^2 - (D_3 + 2D_{66}) \beta_{nj}^2}{D_1 (q_{nj}^2 - \bar{q}_{nj}^2)} \cdot \frac{\phi_{an}^{+j} - (-1)^k \phi_{an}^{-j}}{2} - \frac{1}{D_1 (q_{nj}^2 - \bar{q}_{nj}^2)} \cdot \frac{V_{an}^{+j} - (-1)^k V_{an}^{-j}}{2} \end{aligned} \right\} \quad (32)$$

Proceeding in a similar manner, it is possible to express the undefined constants A_n^{kj} , B_n^{kj} by means of the expansions of the coefficients of boundary values $\phi_y(\pm a, y)$ and $V_x(\pm a, y)$ to give

$$\left. \begin{aligned} A_n^{kj} p_{nk} H_j'(p_{nk} b) &= \frac{D_2 \bar{p}_{nk}^2 - (D_3 + 2D_{66}) \alpha_{nk}^2}{D_2 (\bar{p}_{nk}^2 - p_{nk}^2)} \cdot \frac{\phi_{bn}^{+k} - (-1)^j \phi_{bn}^{-k}}{2} + \frac{1}{D_2 (\bar{p}_{nk}^2 - p_{nk}^2)} \cdot \frac{V_{bn}^{+k} - (-1)^j V_{bn}^{-k}}{2} \\ B_n^{kj} \bar{p}_{nk} H_j'(\bar{p}_{nk} b) &= -\frac{D_2 p_{nk}^2 - (D_3 + 2D_{66}) \alpha_{nk}^2}{D_2 (\bar{p}_{nk}^2 - p_{nk}^2)} \cdot \frac{\phi_{bn}^{+k} - (-1)^j \phi_{bn}^{-k}}{2} - \frac{1}{D_2 (\bar{p}_{nk}^2 - p_{nk}^2)} \cdot \frac{V_{bn}^{+k} - (-1)^j V_{bn}^{-k}}{2} \end{aligned} \right\} \quad (33)$$

Using Eqs. (32) and (33), the amplitude of bending displacement W_{kj} can be written with the help of the Fourier coefficients of $\phi_y(\pm a, y)$, $V_x(\pm a, y)$ and $\phi_x(x, \pm b)$, $V_y(x, \pm b)$ for each case of symmetry to give

$$\begin{aligned} W &= \sum_{k,j=0}^1 \left\{ \sum_{n=1}^{\infty} \left\{ \frac{H_j(p_{nk} y)}{p_{nk} H_j'(p_{nk} b)} \left[(D_2 \bar{p}_{nk}^2 - (D_3 + 2D_{66}) \alpha_{nk}^2) \frac{\phi_{bn}^{+k} - (-1)^j \phi_{bn}^{-k}}{2} + \frac{V_{bn}^{+k} - (-1)^j V_{bn}^{-k}}{2} \right] - \right. \right. \\ &\quad \left. \left. - \frac{H_j(\bar{p}_{nk} y)}{\bar{p}_{nk} H_j'(\bar{p}_{nk} b)} \left[(D_2 p_{nk}^2 - (D_3 + 2D_{66}) \alpha_{nk}^2) \frac{\phi_{bn}^{+k} - (-1)^j \phi_{bn}^{-k}}{2} + \frac{V_{bn}^{+k} - (-1)^j V_{bn}^{-k}}{2} \right] \right\} \frac{T_k(\alpha_{nk} x)}{D_2 (p_{nk}^2 - \bar{p}_{nk}^2)} + \right. \\ &\quad \left. + \left\{ \frac{H_k(q_{nj} x)}{q_{nj} H_j'(q_{nj} a)} \left[(D_1 \bar{q}_{nj}^2 - (D_3 + 2D_{66}) \beta_{nj}^2) \frac{\phi_{an}^{+j} - (-1)^k \phi_{an}^{-j}}{2} + \frac{V_{an}^{+j} - (-1)^k V_{an}^{-j}}{2} \right] - \right. \right. \\ &\quad \left. \left. - \frac{H_k(\bar{q}_{nj} x)}{\bar{q}_{nj} H_j'(\bar{q}_{nj} a)} \left[(D_1 q_{nj}^2 - (D_3 + 2D_{66}) \beta_{nj}^2) \frac{\phi_{an}^{+j} - (-1)^k \phi_{an}^{-j}}{2} + \frac{V_{an}^{+j} - (-1)^k V_{an}^{-j}}{2} \right] \right\} \frac{T_j(\beta_{nj} y)}{D_1 (q_{nj}^2 - \bar{q}_{nj}^2)} \right\} \quad (34) \end{aligned}$$

By making use of Eqs. (17) and (18), the expressions for bending moments M_x and M_y can be written as

$$\begin{aligned} M_x &= \sum_{n=1}^{\infty} \left\{ A_n^{kj} [D_{12} \alpha_{nk}^2 - D_{12} \bar{p}_{nk}^2] H_j(p_{nk} y) \right. \\ &\quad + B_n^{kj} [D_{12} \alpha_{nk}^2 - D_{12} \bar{p}_{nk}^2] H_j(\bar{p}_{nk} y) T_k(\alpha_{nk} x) + \\ &\quad + \sum_{n=1}^{\infty} \left\{ C_n^{kj} [D_{12} \beta_{nj}^2 - D_{12} q_{nj}^2] H_k(q_{nj} x) \right. \\ &\quad \left. + D_n^{kj} [D_{12} \beta_{nj}^2 - D_{12} \bar{q}_{nj}^2] H_k(\bar{q}_{nj} x) T_j(\beta_{nj} y) \right\} \end{aligned} \quad (35)$$

$$\begin{aligned} M_y &= \sum_{n=1}^{\infty} \left\{ A_n^{kj} [D_{12} \alpha_{nk}^2 - D_{12} p_{nk}^2] H_j(p_{nk} y) \right. \\ &\quad + B_n^{kj} [D_{12} \alpha_{nk}^2 - D_{12} \bar{p}_{nk}^2] H_j(\bar{p}_{nk} y) T_k(\alpha_{nk} x) + \\ &\quad + \sum_{n=1}^{\infty} \left\{ C_n^{kj} [D_{12} \beta_{nj}^2 - D_{12} q_{nj}^2] H_k(q_{nj} x) \right. \\ &\quad \left. + D_n^{kj} [D_{12} \beta_{nj}^2 - D_{12} \bar{q}_{nj}^2] H_k(\bar{q}_{nj} x) \beta_{nj} T_j(\beta_{nj} y) \right\} \end{aligned} \quad (36)$$

Clearly, the substitution of the expressions for the undefined coefficients C_n^{kj} , D_n^{kj} and A_n^{kj} , B_n^{kj} from Eqs. (32) and (33) into Eqs. (35), (36) makes it possible to express the bending moments M_x and M_y in terms of the boundary values of the Fourier coefficients of bending rotations and shear forces. Regarding this development, the following relationships are utilized

$$\left. \begin{aligned} \frac{\phi_{an}^{+j} - (-1)^k \phi_{an}^{-j}}{2} &= \phi_{an}^{kj} \\ \frac{\phi_{bn}^{+k} - (-1)^j \phi_{bn}^{-k}}{2} &= \phi_{bn}^{kj} \\ \frac{V_{an}^{+j} - (-1)^k V_{an}^{-j}}{2} &= V_{an}^{kj} \\ \frac{V_{bn}^{+k} - (-1)^j V_{bn}^{-k}}{2} &= V_{bn}^{kj} \end{aligned} \right\} \quad (37)$$

It should be noted that the expressions given by Eq. (37) are the Fourier coefficients of the expansions of trigonometric series related by the following functions

$$\left. \begin{aligned} \phi_a^{kj}(y) &= \frac{\phi_y(a,y) - (-1)^k \phi_y(-a,y) + (-1)^j \phi_y(a,-y) - (-1)^{k+j} \phi_y(-a,-y)}{4} = \sum_{n=1}^{\infty} \phi_{an}^{kj} T_j(\beta_{nj} y) \\ \phi_b^{kj}(x) &= \frac{\phi_x(x,b) - (-1)^j \phi_x(x,-b) + (-1)^k \phi_x(-x,b) - (-1)^{k+j} \phi_x(-x,-b)}{4} = \sum_{n=1}^{\infty} \phi_{bn}^{kj} T_k(\alpha_{nk} x) \\ V_a^{kj}(y) &= \frac{V_x(a,y) - (-1)^k V_x(-a,y) + (-1)^j V_x(a,-y) - (-1)^{k+j} V_x(-a,-y)}{4} = \sum_{n=1}^{\infty} V_{an}^{kj} T_j(\beta_{nj} y) \\ V_b^{kj}(x) &= \frac{V_y(x,b) - (-1)^j V_y(x,-b) + (-1)^k V_y(-x,b) - (-1)^{k+j} V_y(-x,-b)}{4} = \sum_{n=1}^{\infty} V_{bn}^{kj} T_k(\alpha_{nk} x) \end{aligned} \right\} \quad (38)$$

The next step is focused on establishing the relationship between the Fourier coefficients of Eqs. (37)-(38) and the coefficients of $W_{an}^{\pm k}$, $W_{bn}^{\pm k}$, $M_{an}^{\pm k}$, $M_{bn}^{\pm k}$. To achieve this objective, we consider the expressions for W and M_x, M_y at the plate boundaries which are obtainable from the general solution given by Eq. (34). The procedure used is as follows

Substituting $x = \pm a$ in Eq. (34) and using Eq. (9) give the following functional relationships

$$\begin{aligned} W(\pm a, y) &= \sum_{k,j=0}^1 (\pm 1)^k \left\{ \sum_{n=1}^{\infty} \left\{ \frac{H_j(p_{nk} y)}{p_{nk} H_j'(p_{nk} b)} \left[(D_2 \bar{p}_{nk}^2 - (D_3 + 2D_{66}) \alpha_{nk}^2) \phi_{bn}^{kj} + V_{bn}^{kj} \right] - \right. \right. \\ &\quad \left. \left. - \frac{H_j(\bar{p}_{nk} y)}{\bar{p}_{nk} H_j'(\bar{p}_{nk} b)} \left[(D_2 p_{nk}^2 - (D_3 + 2D_{66}) \alpha_{nk}^2) \phi_{bn}^{kj} + V_{bn}^{kj} \right] \right\} \frac{(-1)^{n+k}}{D_2 (p_{nk}^2 - \bar{p}_{nk}^2)} \right. \\ &\quad \left. + \left\{ \frac{H_k(q_{nj} a)}{q_{nj} H_j'(q_{nj} a)} \left[(D_1 \bar{q}_{nj}^2 - (D_3 + 2D_{66}) \beta_{nj}^2) \phi_{an}^{kj} + V_{an}^{kj} \right] \right. \right. \\ &\quad \left. \left. - \frac{H_k(\bar{q}_{nj} a)}{\bar{q}_{nj} H_j'(\bar{q}_{nj} a)} \left[(D_1 q_{nj}^2 - (D_3 + 2D_{66}) \beta_{nj}^2) \phi_{an}^{kj} + V_{an}^{kj} \right] \right\} \frac{T_j(\beta_{nj} y)}{D_1 (q_{nj}^2 - \bar{q}_{nj}^2)} \right\} \\ &= \sum_{j=0}^1 \sum_{n=1}^{\infty} W_{an}^{\pm j} T_j(\beta_{nj} y) \end{aligned} \quad (39)$$

For further transformation of Eqs. (39) we can use the following equality

$$\frac{W(a, y) + (-1)^k W(-a, y)}{2} = \sum_{j=0}^1 \sum_{n=1}^{\infty} \frac{w_{an}^{+j} + (-1)^k w_{an}^{-j}}{2} T_j(\beta_{nj} y) \quad (k = 0, 1) \quad (40)$$

In this way, one can derive representation for each component (k, j) of W separately in the following form

$$\begin{aligned} &\sum_{n=1}^{\infty} \left\{ \frac{H_j(p_{nk} y) \left[(D_2 \bar{p}_{nk}^2 - (D_3 + 2D_{66}) \alpha_{nk}^2) \phi_{bn}^{kj} + V_{bn}^{kj} \right]}{D_2 (\bar{p}_{nk}^2 - p_{nk}^2) p_{nk} H_j'(p_{nk} b)} \right. \\ &\quad \left. - \frac{H_j(\bar{p}_{nk} y) \left[(D_2 p_{nk}^2 - (D_3 + 2D_{66}) \alpha_{nk}^2) \phi_{bn}^{kj} + V_{bn}^{kj} \right]}{(\bar{p}_{nk}^2 - p_{nk}^2) \bar{p}_{nk} H_j'(\bar{p}_{nk} b)} \right\} (-1)^{n+k} \\ &+ \sum_{n=1}^{\infty} \left\{ \frac{H_k(q_{nj} a) \left[(D_1 \bar{q}_{nj}^2 - (D_3 + 2D_{66}) \beta_{nj}^2) \phi_{an}^{kj} + V_{an}^{kj} \right]}{q_{nj} H_j'(q_{nj} a)} \right. \\ &\quad \left. - \frac{H_k(\bar{q}_{nj} a) \left[(D_1 q_{nj}^2 - (D_3 + 2D_{66}) \beta_{nj}^2) \phi_{an}^{kj} + V_{an}^{kj} \right]}{\bar{q}_{nj} H_j'(\bar{q}_{nj} a)} \right\} \frac{T_j(\beta_{nj} y)}{D_1 (q_{nj}^2 - \bar{q}_{nj}^2)} = \\ &= \sum_{n=1}^{\infty} \frac{W_{an}^{+j} + (-1)^k W_{an}^{-j}}{2} T_j(\beta_{nj} y) \end{aligned} \quad (41)$$

In the algebraic functional given in Eq. (41), we now utilize the expansion of the hyperbolic functions $H_j(py)$ in terms of the trigonometric functions $\{T_j(\beta_{nj} y)\}$ according to well-known relationships which can be found in the mathematical literature [49]. Thus, the expansion of the trigonometric and hyperbolic functions can be related as follows

$$\frac{H_j(py)}{H'_j(pb)} = \frac{p}{b} \sum_{m=1}^{\infty} \frac{(-1)^{m+1} (2 - \delta_{j0} \delta_{1m})}{\beta_{mj}^2 + p^2} T_j(\beta_{mj}y) \quad (42)$$

where δ_{sj} is the usual Kronecker delta which is 1 if integer s and l coincides and equal to 0 otherwise.

Substituting Eq. (42) into Eqs. (41) and changing the order of summation for the double series, we obtain after some algebraic transformations, the first part of equations of the infinite linear system which connects the Fourier coefficients to the boundary values of the plate as follows

$$\begin{aligned} \frac{2-\delta_{j0}\delta_{1m}}{bD_1} \sum_{n=1}^{\infty} (-1)^{n+m} \frac{(D_2\beta_{mj}^2 + D_{12}\alpha_{nk}^2)\phi_{bn}^{kj} + V_{bn}^{kj}}{(\alpha_{nk}^2 + q_{mj}^2)(\alpha_{nk}^2 + \bar{q}_{mj}^2)} + \frac{H_k(q_{mj}a)}{H'_k(q_{mj}a)} \cdot \frac{D_1\bar{q}_{mj}^2 - (D_3 + 2D_{66})\beta_{mj}^2}{q_{mj}(\bar{q}_{mj}^2 - q_{mj}^2)} - \\ \frac{H_k(\bar{q}_{mj}a)}{H'_k(\bar{q}_{mj}a)} \cdot \frac{D_1q_{mj}^2 - (D_3 + 2D_{66})\beta_{mj}^2}{q_{mj}(q_{mj}^2 - \bar{q}_{mj}^2)} \frac{\phi_{am}^{kj}}{D_1} + \left(\frac{q_{mj}H'_k(q_{mj}a)}{H_k(q_{mj}a)} - \frac{\bar{q}_{mj}H'_k(\bar{q}_{mj}a)}{H_k(\bar{q}_{mj}a)} \right) \frac{V_{am}^{kj}}{D_1(q_{mj}^2 - \bar{q}_{mj}^2)} \\ = \frac{W_{am}^{+j} + (-1)^k W_{am}^{-j}}{2} \end{aligned} \quad (m = 1, 2, \dots) \quad (43)$$

In a similar manner, we consider the boundary value relationships for $W(x, \pm b)$, $M_x(\pm a, y)$ and $M_y(x, \pm b)$ to obtain the rest part of the equations for the linear system. Introducing the following notations for convenience

$$\left. \begin{aligned} \frac{W_{am}^{+j} + (-1)^k W_{am}^{-j}}{2} &= W_{an}^{kj} \\ \frac{W_{bn}^{+k} + (-1)^j W_{bn}^{-k}}{2} &= W_{bn}^{kj} \\ \frac{M_{an}^{+j} + (-1)^k M_{an}^{-j}}{2} &= M_{an}^{kj} \\ \frac{M_{bn}^{+k} + (-1)^j M_{bn}^{-k}}{2} &= M_{bn}^{kj} \end{aligned} \right\} \quad (44)$$

the infinite system of linear algebraic equations can be written as

$$\begin{aligned} \frac{2 - \delta_{j0}\delta_{1m}}{bD_1} \sum_{n=1}^{\infty} (-1)^{n+m} \frac{(D_2\beta_{mj}^2 + D_{12}\alpha_{nk}^2)\phi_{bn}^{kj} + V_{bn}^{kj}}{(\alpha_{nk}^2 + q_{mj}^2)(\alpha_{nk}^2 + \bar{q}_{mj}^2)} + \Delta_m^1 \phi_{am}^{kj} \\ + \Delta_m^2 V_{am}^{kj} = W_{am}^{kj} \end{aligned} \quad (45)$$

$$\begin{aligned} \frac{2-\delta_{j0}\delta_{1m}}{bD_1} \sum_{n=1}^{\infty} (-1)^{n+m} \frac{(D_3 - 4D_{66}^2 - D_1D_2)\beta_{mj}^2\alpha_{nk}^2 - D_1D\Omega^4}{(\alpha_{nk}^2 + q_{mj}^2)(\alpha_{nk}^2 + \bar{q}_{mj}^2)} \phi_{bn}^{kj} - (D_{12}\beta_{mj}^2 + D_1\alpha_{nk}^2) \frac{V_{bn}^{kj}}{b} + \\ + \Delta_m^3 \phi_{am}^{kj} + \Delta_m^4 V_{am}^{kj} = -M_{an}^{kj} \end{aligned} \quad (46)$$

$$\frac{2 - \delta_{k0}\delta_{1m}}{aD_2} \sum_{n=1}^{\infty} (-1)^{n+m} \frac{(D_1\alpha_{mk}^2 + D_{12}\beta_{nj}^2)\phi_{an}^{kj} + V_{an}^{kj}}{(\beta_{nj}^2 + p_{mk}^2)(\beta_{nj}^2 + \bar{p}_{mk}^2)} + \Delta_m^5 \phi_{bm}^{kj} + \Delta_m^6 V_{bm}^{kj} = W_{bm}^{kj} \quad (47)$$

$$\begin{aligned} \frac{2-\delta_{k0}\delta_{1m}}{aD_2} \sum_{n=1}^{\infty} (-1)^{n+m} \frac{(D_3 - 4D_{66}^2 - D_1D_2)\beta_{nj}^2\alpha_{mk}^2 - D_1D\Omega^4}{(\beta_{nj}^2 + p_{mk}^2)(\beta_{nj}^2 + \bar{p}_{mk}^2)} \phi_{an}^{kj} - (D_{12}\alpha_{mk}^2 + D_2\beta_{nj}^2) \frac{V_{an}^{kj}}{a} + \\ + \Delta_m^7 \phi_{bm}^{kj} + \Delta_m^8 V_{bm}^{kj} = -M_{bm}^{kj} \end{aligned} \quad (48)$$

$m = 1, 2, \dots$

where we now introduce the notation

$$Cth_k(z) = \frac{H_k(z)}{H'_k(z)} \quad (49)$$

and

$$\left. \begin{aligned} D_1\Delta_m^1 &= \frac{D_1\bar{q}_{mj}^2 - (D_3 + 2D_{66})\beta_{mj}^2}{q_{mj}(q_{mj}^2 - \bar{q}_{mj}^2)} Cth_k(q_{mj}a) - \frac{D_1q_{mj}^2 - (D_3 + 2D_{66})\beta_{mj}^2}{q_{mj}(q_{mj}^2 - \bar{q}_{mj}^2)} Cth_k(\bar{q}_{mj}a); \\ D_1\Delta_m^2 &= \frac{1}{(q_{mj} - \bar{q}_{mj})} \left(\frac{Cth_k(q_{mj}a)}{q_{mj}} - \frac{Cth_k(\bar{q}_{mj}a)}{\bar{q}_{mj}} \right) \\ D_1\Delta_m^3 &= \frac{(D_1\bar{q}_{mj}^2 - (D_3 + 2D_{66})\beta_{mj}^2)(D_1q_{mj}^2 - D_{12}\beta_{mj}^2)}{q_{mj}(q_{mj}^2 - \bar{q}_{mj}^2)} Cth_k(q_{mj}a) - \\ &\quad - \frac{(D_1q_{mj}^2 - (D_3 + 2D_{66})\beta_{mj}^2)(D_1\bar{q}_{mj}^2 - D_{12}\beta_{mj}^2)}{q_{mj}(q_{mj}^2 - \bar{q}_{mj}^2)} Cth_k(\bar{q}_{mj}a); \\ D_1\Delta_m^4 &= \frac{D_1q_{mj}^2 - D_{12}\beta_{mj}^2}{q_{mj}(q_{mj}^2 - \bar{q}_{mj}^2)} Cth_k(q_{mj}a) - \frac{D_1\bar{q}_{mj}^2 - D_{12}\beta_{mj}^2}{\bar{q}_{mj}(q_{mj}^2 - \bar{q}_{mj}^2)} Cth_k(\bar{q}_{mj}a); \\ D_2\Delta_m^5 &= \frac{D_2p_{mk}^2 - (D_3 + 2D_{66})\alpha_{mk}^2}{p_{mk}(p_{mk}^2 - \bar{p}_{mk}^2)} Cth_j(p_{mk}b) - \frac{D_2\bar{p}_{mk}^2 - (D_3 + 2D_{66})\alpha_{mk}^2}{\bar{p}_{mk}(p_{mk}^2 - \bar{p}_{mk}^2)} Cth_j(\bar{p}_{mk}b); \\ D_2\Delta_m^6 &= \frac{1}{(p_{mk} - \bar{p}_{mk})} \left(\frac{Cth_j(p_{mk}b)}{p_{mk}} - \frac{Cth_j(\bar{p}_{mk}b)}{\bar{p}_{mk}} \right) \\ D_2\Delta_m^7 &= \frac{(D_2p_{mk}^2 - (D_3 + 2D_{66})\alpha_{mk}^2)(D_2\bar{p}_{mk}^2 - D_{12}\alpha_{mk}^2)}{p_{mk}(p_{mk}^2 - \bar{p}_{mk}^2)} Cth_j(p_{mk}b) - \\ &\quad - \frac{(D_2\bar{p}_{mk}^2 - (D_3 + 2D_{66})\alpha_{mk}^2)(D_2p_{mk}^2 - D_{12}\alpha_{mk}^2)}{\bar{p}_{mk}(p_{mk}^2 - \bar{p}_{mk}^2)} Cth_j(\bar{p}_{mk}b); \\ D_2\Delta_m^8 &= \frac{D_2p_{mk}^2 - D_{12}\alpha_{mk}^2}{p_{mk}(p_{mk}^2 - \bar{p}_{mk}^2)} Cth_j(p_{mk}b) - \frac{D_2\bar{p}_{mk}^2 - D_{12}\alpha_{mk}^2}{\bar{p}_{mk}(p_{mk}^2 - \bar{p}_{mk}^2)} Cth_j(\bar{p}_{mk}b); \end{aligned} \right\} \quad (50)$$

Thus Eqs. (45)–(48) establish the dependency between the boundary values of forces and displacements for the plate element which is essentially its dynamic stiffness matrix with line nodes represented by its edges. The exact formulation of the problem has infinite terms in the series, but for practical purposes, the infinite dynamic stiffness matrix can be approximated to a finite dynamic stiffness matrix using a finite number of terms in the series and the results can be computed sufficiently accurately, even up to machine accuracy [38,40,42].

It should be also noted that in the above derivations, the introduced coefficients of W_{an}^{kj} , W_{bn}^{kj} , M_{an}^{kj} and M_{bn}^{kj} are Fourier coefficients relating the following functions

$$\left. \begin{aligned} W_a^{kj}(y) &= \frac{W(a,y) + (-1)^k W(-a,y) + (-1)^j W(a,-y) + (-1)^{k+j} W(-a,-y)}{4} = \sum_{n=1}^{\infty} W_{an}^{kj} T_j(\beta_{nj}y) \\ W_b^{kj}(x) &= \frac{W(x,b) + (-1)^j W(x,-b) + (-1)^k W(-x,b) + (-1)^{k+j} W(-x,-b)}{4} = \sum_{n=1}^{\infty} W_{bn}^{kj} T_k(\alpha_{nk}x) \\ M_a^{kj}(y) &= \frac{M_x(a,y) + (-1)^k M_x(-a,y) + (-1)^j M_x(a,-y) + (-1)^{k+j} M_x(-a,-y)}{4} = \sum_{n=1}^{\infty} M_{an}^{kj} T_j(\beta_{nj}y) \\ M_b^{kj}(x) &= \frac{M_y(x,b) + (-1)^j M_y(x,-b) + (-1)^k M_y(-x,b) + (-1)^{k+j} M_y(-x,-b)}{4} = \sum_{n=1}^{\infty} M_{bn}^{kj} T_k(\alpha_{nk}x) \end{aligned} \right\} \quad (51)$$

3. Dynamic stiffness formulation for a plate element with point nodes

Based on the material presented in Section 2 above, we now derive the dynamic stiffness matrix of the plate with nodal points. Let the boundary functions $W_a^{kj}(y)$, $W_b^{kj}(x)$, $\phi_a^{kj}(y)$, $\phi_b^{kj}(x)$ and $M_a^{kj}(y)$, $M_b^{kj}(x)$, $V_a^{kj}(y)$, $V_b^{kj}(x)$ which are included in the above dynamic stiffness formulation be given their values at some specific node points. Depending on the type of symmetry (Note that according to the introduced notation, the index $k = 0$ corresponds to an even function of the coordinate x , whereas $k = 1$ to an odd function of the same coordinate.), we choose $(N - 1 + k)$ nodes on the segment $[0; a]$ of the x coordinate which satisfy the following nonlinear dependence

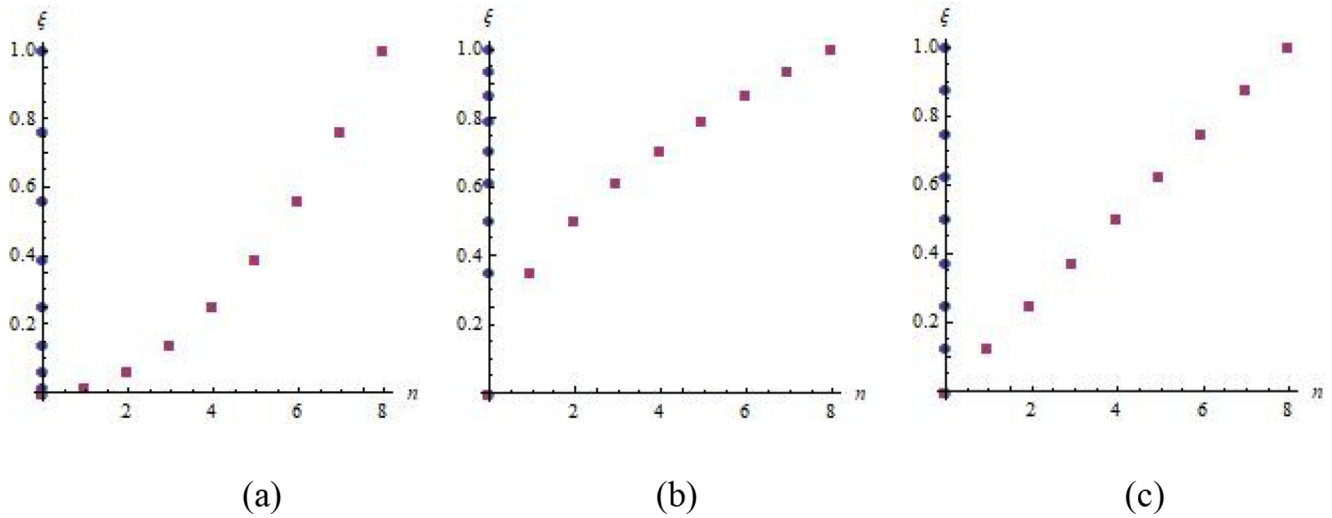


Fig. 2. Different arrangement of nodal points on plate edge.

$$x_n = \frac{\tau(n)}{\tau(N)} a \tag{52}$$

where function $\tau(x)$ is defined on the segment $[0; a]$ which is a monotonically increasing function of x with $\tau(0) = 0$.

For the case of equally spaced nodes $\tau(x) = x$, we can define the following node points

$$\text{For } k = 0 : x_0 = 0, x_1 = \frac{a}{N}, x_2 = \frac{2a}{N}, \dots, x_N = a \tag{53}$$

$$\text{For } k = 1 : x_1 = \frac{a}{N}, x_2 = \frac{2a}{N}, \dots, x_N = a$$

We now consider three different cases of the function $\tau(\xi)$ and Fig. 2 illustrates the mesh of node distribution and its dependency on the function $\tau(\xi)$ for the three cases in non-dimensional form where $\xi = x/a$. In Fig. 2(a), $\tau(\xi) = \xi^2$ where the node spacing arrangement is such that there is more concentration of nodes at the start of the segment, i.e., near $\xi = 0$. By contrast, $\tau(\xi) = \sqrt{\xi}$ in Fig. 2(b) corresponds to node spacing arrangement more concentrated towards the end of the segment, i.e. near $\xi = 1$. Equally spaced arrangement of nodes for which $\tau(\xi) = \xi$ is illustrated in Fig. 2(c).

In a similar manner, let the functions of the coordinate in Y -direction are given in terms of node points on the segment $[0; b]$ with $(N - 1 + j)$ nodes so that

$$y_l = \frac{\tau(l)}{\tau(N)} b, \quad (l = j, j + 1, \dots, N) \tag{54}$$

The boundary displacements for the kj component of the plate are defined as

$$d_N = \left(\{W_a^{kj}(y_l)\}, \{\phi_a^{kj}(y_l)\}, \{W_b^{kj}(x_s)\}, \{\phi_b^{kj}(x_s)\} \right) \tag{55}$$

$(l = j, j + 1, \dots, N; s = k, k + 1, \dots, N)$

The corresponding boundary forces are

$$f_N = \left(\{M_a^{kj}(y_l)\}, \{V_a^{kj}(y_l)\}, \{M_b^{kj}(x_s)\}, \{V_b^{kj}(x_s)\} \right) \tag{56}$$

$(l = j, j + 1, \dots, N; s = k, k + 1, \dots, N)$

From the given data points given by Eqs.(52) and (41), we construct interpolation trigonometric polynomials of functions of the coordinate x with respect to the system of functions $\{T_k(\alpha_{nk}x)\}_{n=1}^{N+1-k}$ and for the functions of the coordinate y , the sys-

tem of functions $\{T_j(\beta_{nj}y)\}_{n=1}^{N+1-j}$ is used. Thus, an approximate, but sufficiently accurate representation of the deflection function $W_a^{kj}(y)$ can be written as

$$W_a^{kj}(y) \approx W_{aN}^{kj}(y) = \sum_{m=1}^{N+1-j} W_{am,N}^{kj} T_j(\beta_{mj}y) \tag{57}$$

where coefficients $W_{am,N}^{kj}$ are now calculated by using the method of least squares. This is probably the best possible representation of the function $\{W_a^{kj}(y_l)\}$ when it is defined at a point in the space of square-integrable functions [50] as in the present case. In fact, such a procedure correlates the mapping of a sequence of real numbers $\{W_a^{kj}(y_l)\}$ to a sequence of real numbers $\{W_{am,N}^{kj}\}$. Such a mapping in the mathematical literature is not uncommon and is usually called the discrete Fourier transform (DFT). The DFT of various types have been widely applied to solve many practical problems, especially in signal theory and information processing. It should be noted that the DFT for the introduced system of trigonometric functions $\{T_j(\beta_{nj}y)\}_{n=1}^{N+1-j}$ has not featured in the existing literature before, and therefore, necessary formulations for the forward and inverse DFT for the present case are briefly described below.

To calculate the coefficients $W_{am,N}^{kj}$ in Eq. (57) by applying the method of least squares necessitated the need to solve the following minimization problem.

$$\text{Minimise } \sum_{n=j}^N \left(W_a^{kj}(y_n) - W_{aN}^{kj}(y_n) \right)^2 \tag{58}$$

Following standard technique (for example, see [51]) to solve the minimization problem described by Eq. (58) leads to the following system of linear equations (known as the normal equations) which determine the Fourier coefficients.

$$\sum_{n=j}^N \left(\sum_{m=1}^{N+1-j} W_{am,N}^{kj} T_j(\beta_{mj}y_n) - W_a^{kj}(y_n) \right) T_j(\beta_{lj}y_n) = 0 \tag{59}$$

$(l = 1, 2, \dots, N + j - 1)$

or,

$$\sum_{m=1}^{N+1-j} M_{lm}^j W_{am,N}^{kj} = \sum_{n=j}^N T_j(\beta_{lj}y_n) W_a^{kj}(y_n) \tag{60}$$

where

$$M_{lm}^j = \sum_{n=j}^N T_j(\beta_{lj}y_n)T_j(\beta_{lm}y_n) \quad (61)$$

The derivation of explicit expressions for the displacement at node points using forward and inverse DFT in the case of equally spaced nodal arrangement is possible because of the exact summation of elements of the matrix $\mathbf{M} = \{M_{lm}^j\}_{l,m=1}^{N+1-j}$, which ultimately allows us to build analytically an inverse matrix

$$\sigma = \mathbf{M}^{-1} \quad (62)$$

The matrix σ can now be constructed for any value of the problem parameter that satisfies the requirement of the existence of the direct and inverse mapping of DFT between $\{W_a^{kj}(y_l)\}$ and $\{W_{am,N}^{kj}\}$, see Appendix A. Furthermore, the known elements σ_{lm}^j of matrix σ in Eq. (62) allow us to write explicit expressions for the inverse transform as follows

$$W_{am,N}^{kj} = \sum_{n=j}^N \left\{ \sum_{l=1}^{N+1-j} \sigma_{ml}^j T_j(\beta_{lj}y_n) \right\} W_a^{kj}(y_n) \quad (63)$$

Since the interpolation trigonometric polynomial $W_{aN}^{kj}(y)$ at the nodes takes on the given values $W_{aN}^{kj}(y_n) = W_a^{kj}(y_n)$, the introduction of the following notation is useful

$$F_{mn}^j = \sum_{l=1}^{N+1-j} \sigma_{ml}^j T_j(\beta_{lj}y_n) \quad (64)$$

In this way, we obtain the expressions for the forward and inverse DFT as given below

$$W_a^{kj}(y_n) = \sum_{m=1}^{N+1-j} T_j(\beta_{mj}y_n) W_{am,N}^{kj} \quad (65)$$

$$W_{am,N}^{kj} = \sum_{n=j}^N F_{mn}^j W_a^{kj}(y_n) \quad (66)$$

It should be also noted that summation in Eq. (64) allows trigonometric (analytical) summation. This will prove useful when increasing the computational efficiency within the inverse transform Eq. (66) for large values of the number N .

In a similar way, interpolation trigonometric polynomials can be constructed for the rest of the boundary displacements and forces. Let these interpolation trigonometric polynomials are denoted by

$$\left. \begin{aligned} W_{aN}^{kj}(y) &= \sum_{m=1}^{N+1-j} W_{am,N}^{kj} T_j(\beta_{mj}y), & W_{bN}^{kj}(x) &= \sum_{m=1}^{N+1-k} W_{bm,N}^{kj} T_k(\alpha_{mk}x) \\ \phi_{aN}^{kj}(y) &= \sum_{m=1}^{N+1-j} \phi_{am,N}^{kj} T_j(\beta_{mj}y), & \phi_{bN}^{kj}(x) &= \sum_{m=1}^{N+1-k} \phi_{bm,N}^{kj} T_k(\alpha_{mk}x) \end{aligned} \right\} \quad (67)$$

and

$$\left. \begin{aligned} M_{aN}^{kj}(y) &= \sum_{m=1}^{N+1-j} M_{am,N}^{kj} T_j(\beta_{mj}y), & M_{bN}^{kj}(x) &= \sum_{m=1}^{N+1-k} M_{bm,N}^{kj} T_k(\alpha_{mk}x) \\ V_{aN}^{kj}(y) &= \sum_{m=1}^{N+1-j} V_{am,N}^{kj} T_j(\beta_{mj}y), & V_{bN}^{kj}(x) &= \sum_{m=1}^{N+1-k} V_{bm,N}^{kj} T_k(\alpha_{mk}x) \end{aligned} \right\} \quad (68)$$

where coefficients of Eqs. (67) and (68) are calculated by using an analogy to Eq. (66) for the given values of the functions at the nodal points (see Eqs. (52) and (55)). Thus, the polynomials for the displacements and forces are given by

Displacements:

$$\left. \begin{aligned} W_{am,N}^{kj} &= \sum_{n=j}^N F_{mn}^j W_a^{kj}(y_n), & W_{bm,N}^{kj} &= \sum_{n=j}^N F_{mn}^k W_b^{kj}(x_n) \\ \phi_{am,N}^{kj} &= \sum_{n=j}^N F_{mn}^j \phi_a^{kj}(y_n), & \phi_{bm,N}^{kj} &= \sum_{n=j}^N F_{mn}^k \phi_b^{kj}(x_n) \end{aligned} \right\} \quad (69)$$

Forces:

$$\left. \begin{aligned} M_{am,N}^{kj} &= \sum_{n=j}^N F_{mn}^j M_a^{kj}(y_n), & M_{bm,N}^{kj} &= \sum_{n=j}^N F_{mn}^k M_b^{kj}(x_n) \\ V_{am,N}^{kj} &= \sum_{n=j}^N F_{mn}^j V_a^{kj}(y_n), & V_{bm,N}^{kj} &= \sum_{n=j}^N F_{mn}^k V_b^{kj}(x_n) \end{aligned} \right\} \quad (70)$$

From the theory of Fourier series [50], it can be ascertained that the coefficients of interpolation trigonometric polynomials of Eqs. (69) and (70) will tend to reach their exact values through their Fourier coefficients when $N \rightarrow \infty$.

Now the substitution of the expressions in Eqs. (69) and (70) into Eqs. (45)-(48) leads to the resulting dynamic stiffness matrix comprising $2 \times (2N + 2 - k - j)$ equations which relate the boundary forces and displacements at nodal points. The required equations which lead to the dynamic stiffness matrix can be written as

$$\begin{aligned} & \sum_{n=k}^N \frac{2-\delta_{j0}\delta_{1m}}{bD_1} \sum_{l=1}^{N+1-k} (-1)^{l+m} \frac{(D_2\beta_{mj}^2 + D_{12}\alpha_{lk}^2) F_{ln}^k}{(\alpha_{lk}^2 + q_{mj}^2)(\alpha_{lk}^2 + q_{mj}^2)} \phi_b^{kj}(x_n) + \sum_{n=j}^N \Delta_m^1 F_{mn}^j \phi_a^{kj}(y_n) + \\ & \sum_{n=k}^N \frac{2-\delta_{j0}\delta_{1m}}{bD_1} \sum_{l=1}^{N+1-k} \frac{(-1)^{l+m} F_{ln}^k}{(\alpha_{lk}^2 + q_{mj}^2)(\alpha_{lk}^2 + q_{mj}^2)} V_b^{kj}(x_n) + \sum_{n=j}^N \Delta_m^2 F_{mn}^j V_a^{kj}(y_n) = \sum_{n=j}^N F_{mn}^j W_a^{kj}(y_n) \end{aligned} \quad (71)$$

$$\begin{aligned} & \sum_{n=k}^N \frac{2-\delta_{j0}\delta_{1m}}{bD_1} \sum_{l=1}^{N+1-k} (-1)^{l+m} \frac{(D_3^2 - 4D_6^2 - D_1D_2)\beta_{mj}^2\alpha_{lk}^2 - D_1D\Omega^4}{(\alpha_{lk}^2 + q_{mj}^2)(\alpha_{lk}^2 + q_{mj}^2)} F_{ln}^k \phi_b^{kj}(x_n) \\ & + \sum_{n=j}^N \Delta_m^3 F_{mn}^j \phi_a^{kj}(y_n) - \sum_{n=k}^N \frac{2-\delta_{j0}\delta_{1m}}{bD_1} \sum_{l=1}^{N+1-k} (-1)^{l+m} \frac{(D_{12}\beta_{mj}^2 + D_1\alpha_{lk}^2) F_{ln}^k}{(\alpha_{lk}^2 + q_{mj}^2)(\alpha_{lk}^2 + q_{mj}^2)} V_b^{kj}(x_n) \\ & + \sum_{n=j}^N \Delta_m^4 F_{mn}^j V_a^{kj}(y_n) = - \sum_{n=j}^N F_{mn}^j M_a^{kj}(y_n) \end{aligned} \quad (72)$$

($m = 1, 2, \dots, N + 1 - j$).

$$\begin{aligned} & \sum_{n=j}^N \frac{2-\delta_{j0}\delta_{1m}}{aD_2} \sum_{l=1}^{N+1-j} (-1)^{l+m} \frac{(D_1\alpha_{mk}^2 + D_{12}\beta_{lj}^2) F_{ln}^j}{(\beta_{lj}^2 + p_{mk}^2)(\beta_{lj}^2 + p_{mk}^2)} \phi_a^{kj}(y_n) + \sum_{n=k}^N \Delta_m^5 F_{mn}^k \phi_b^{kj}(x_n) + \\ & + \sum_{n=j}^N \frac{2-\delta_{j0}\delta_{1m}}{aD_2} \sum_{l=1}^{N+1-j} \frac{(-1)^{l+m} F_{ln}^j}{(\beta_{lj}^2 + p_{mk}^2)(\beta_{lj}^2 + p_{mk}^2)} V_a^{kj}(y_n) + \sum_{n=k}^N \Delta_m^6 F_{mn}^k V_b^{kj}(x_n) = \sum_{n=k}^N F_{mn}^k W_b^{kj}(x_n) \end{aligned} \quad (73)$$

$$\begin{aligned} & \sum_{n=j}^N \frac{2-\delta_{j0}\delta_{1m}}{aD_2} \sum_{l=1}^{N+1-j} (-1)^{l+m} \frac{(D_3^2 - 4D_6^2 - D_1D_2)\beta_{lj}^2\alpha_{mk}^2 - D_1D\Omega^4}{(\beta_{lj}^2 + p_{mk}^2)(\beta_{lj}^2 + p_{mk}^2)} F_{ln}^j \phi_a^{kj}(y_n) \\ & + \sum_{n=k}^N \Delta_m^7 F_{mn}^k \phi_b^{kj}(x_n) - \sum_{n=j}^N \frac{2-\delta_{j0}\delta_{1m}}{aD_2} \sum_{l=1}^{N+1-j} (-1)^{l+m} \frac{(D_{12}\alpha_{mk}^2 + D_2\beta_{lj}^2) F_{ln}^j}{(\beta_{lj}^2 + p_{mk}^2)(\beta_{lj}^2 + p_{mk}^2)} V_a^{kj}(y_n) \\ & + \sum_{n=k}^N \Delta_m^8 F_{mn}^k V_b^{kj}(x_n) = - \sum_{n=k}^N F_{mn}^k M_b^{kj}(x_n) \end{aligned} \quad (74)$$

($m = 1, 2, \dots, N + 1 - k$).

($k, j = 0, 1$).

Finally, by considering the dependency between the set represented by Eqs. (38) and (41) and the set of boundary conditions for forces and displacements represented by Eq. (8) evaluated at the nodal points, we arrive at the following relationship

$$\left. \begin{aligned}
 4W_a^{kj}(y_n) &= W(a, y_n) + (-1)^k W(-a, y_n) + (-1)^j W(a, -y_n) + (-1)^{k+j} W(-a, -y_n) \\
 4W_b^{kj}(x_n) &= W(x_n, b) + (-1)^j W(x_n, -b) + (-1)^k W(-x_n, b) + (-1)^{k+j} W(-x_n, -b) \\
 4\phi_a^{kj}(y_n) &= \phi_y(a, y_n) - (-1)^k \phi_y(-a, y_n) + (-1)^j \phi_y(a, -y_n) - (-1)^{k+j} \phi_y(-a, -y_n) \\
 4\phi_b^{kj}(x_n) &= \phi_x(x_n, b) - (-1)^j \phi_x(x_n, -b) + (-1)^k \phi_x(-x_n, b) - (-1)^{k+j} \phi_x(-x_n, -b) \\
 4M_a^{kj}(y_n) &= M_x(a, y_n) + (-1)^k M_x(-a, y_n) + (-1)^j M_x(a, -y_n) + (-1)^{k+j} M_x(-a, -y_n) \\
 4M_b^{kj}(x_n) &= M_y(x_n, b) + (-1)^j M_y(x_n, -b) + (-1)^k M_y(-x_n, b) + (-1)^{k+j} M_y(-x_n, -b) \\
 4V_a^{kj}(y_n) &= V_x(a, y_n) - (-1)^k V_x(-a, y_n) + (-1)^j V_x(a, -y_n) - (-1)^{k+j} V_x(-a, -y_n) \\
 4V_b^{kj}(x_n) &= V_y(x_n, b) - (-1)^j V_y(x_n, -b) + (-1)^k V_y(-x_n, b) - (-1)^{k+j} V_y(-x_n, -b)
 \end{aligned} \right\} \quad (75)$$

Clearly, by substituting Eq. (75) into the system of Eqs. (71)–(74) for all of the four cases of symmetry (kj), one can obtain dependency between the point-defined components f and d in Eq. (8). Thus, Eqs. (71)–(74) together with Eq. (75) describe the dynamic stiffness matrix of the plate element, relating the forces and displacements at the nodal points defined at the plate boundaries.

4. Numerical results and discussion

The method developed above has been implemented in a computer program using Mathematica. It is helpful to explain briefly how the results were obtained. As can be seen in Section 3 above, the system of Eqs. (71)–(74) connects the values of the boundary forces and boundary displacements at any nodal points of the plate edges. Thus, to set the boundary conditions on some edges of the plate or on some parts of the edges of the plate, it is sufficient to assign the values of the boundary functions at the nodal points of the corresponding edge. The connection between two or more plate elements can be carried out in a similar way. When two or more plates are joined together, the values of the boundary displacements and boundary forces are coincident at the nodal points on the common part or parts of the plate. The values of boundary displacements and boundary forces at the nodal points given by Eqs. (71)–(74) that are not involved in the boundary conditions, are the unknown variables. The system of linear equations is formed relative to these unknown variables. The determinant of this system will give the characteristic equation to determine the natural frequencies of the plate comprising nodal plates, but better still, the application of the Wittrick-Williams algorithm [2] to the ensuing dynamic stiffness matrix is a robust solution technique which avoids the cumbersome determinant evaluation that can be sometimes prone to ill-conditioning and also can miss natural frequencies while stepping through the frequencies. The algorithm has been used in this paper in obtaining the results, but some results were checked using the frequency-determinant plot. The corresponding eigenvectors i.e., mode shapes, were recovered in the usual way by assigning an arbitrary displacement to a carefully chosen node and then determining the rest of the displacements in terms of the chosen one. A point is to be made here that the Fourier coefficients corresponding to the mode shapes are determined with the help of Eqs. (69)–(70) for final substitution into Eq. (34).

The first set of results was obtained to assess the convergence performance of the current theory by artificially using point nodes to represent the line nodes which are essentially the edges of the plate. This approach is suitable because comparison of results with those readily available in the literature [1,4,5,22,23,38,42] for plates modelled by line nodes is easy and straightforward. Thus, using the developed theory, the line nodes are modelled by N number of point nodes on each edge of the plate. With increasing values of the number of nodal points N , Tables 1–3 show the first ten non-dimensional natural frequencies computed using current theory for three different boundary conditions of the plate which are Free-Free-Free-Free (FFFF), Clamped-Clamped-Clamped-Clamped (CCCC) and Clamped-Free-Clamped-Free (CFCF), respectively

alongside the published results [42] shown in the last column of these tables. For each case, three different node-point distributions on the plate edges, represented by $\tau(\xi)$ (see underneath Eq. (53) and Fig. 2) have been used in the present theory. The results for the first ten non-dimensional natural frequencies (Ω_n) from the present theory when compared with the published results given in the last column show excellent agreement for all three boundary conditions of the plate, which confirms the correctness of the theory. (Note that $N = 32$ gives extremely close results even up to machine accuracy as given by line nodes.) As can be seen from the results shown in Tables 1–3 that for classical boundary conditions FFFF, CCCC and CFCF, even with 4 nodal points on each side of the plate, the first ten natural frequencies can be computed very accurately. The discrepancy with exact results is astonishingly small, being within 0.5%. An analysis of the symmetry and antisymmetry of the modes show that more rapid convergence is observed for the fundamental mode (i.e. the first mode) in all cases. It has already been noted from the results given by Tables 1–3 that 4 nodal points are sufficient for good accuracy, however, for the antisymmetric modes it is possible to find the values of the fundamental natural frequencies with an accuracy of three significant figures even with $N = 2$. The investigation has shown that for higher symmetric modes, the convergence of results is somewhat inferior, wherein the use of non-equally spaced mesh for the nodes gives better result, see for example Ω_7 for the FFFF case in Table 1, and Ω_3 and Ω_8 for the CFCF case in Table 3. Nevertheless, even for these cases, the use of $N = 8$ for the number of nodal points, makes it possible to achieve very accurate results for the natural frequencies.

For further verification and validation of results, the first five natural frequencies of an isotropic plate with CFFF boundary conditions are computed using the present theory and they are compared with those reported in the literature [34] using SEM and FEM, respectively. The comparative results are shown in Table 4. Note that N_{SEM} in Table 4 is the number of series terms in the representation of the shape functions in SEM [34]. Given the similarities between DSM and SEM, it can be seen from Table 4 that the results using the proposed theory converge almost in the same way as the approach used in SEM [34]. Applying the present theory, 16 nodes to represent half-length of each side of the plate is enough to achieve sufficient accuracy, as can be seen.

As noted earlier, the DSM approach has been repeatedly described in the literature as the most accurate and reliable approach when solving free vibration problems for structures and structural elements. However, for plates, there existed a severe limitation in DSM that line nodes must be used to represent the edges of the plate. Evidently, the work on DSM for plates with point nodes was non-existent until now when the current investigation has successfully overcome this limitation. Therefore, the next set of results was obtained to check the convergence of results using the proposed theory when the boundary conditions are discontinuous and/or partially specified. Table 5 shows the fundamental natural frequency of an isotropic square plate with simple supported boundary condition on its three edges, but the plate is partially clamped at the center of the fourth edge, see Fig. 3. Note that $2a$ is the length of each side of the plate and $2l$ is the portion of length located in the middle of one of the sides of the plate over which the nodal points are distributed. Clearly $l/a = 0$ corresponds to the case when the edge is simply supported, representing SSSS boundary conditions whereas $l/a = 1$ corresponds to the case when the edge is fully clamped, representing SSSC boundary conditions. Comparative results for this problem are available in the literature [4,5] from which the data were taken for the analysis. When computing the fundamental natural frequency of the plate from the present theory, a non-uniform mesh for the node distribution given by $\tau = x^2$ (Fig. 2(a)) with $N = 16$ was used with the node con-

Table 1

Convergence of results for a square orthotropic plate with FFFF boundary condition using the present method with different mesh distribution of nodes represented by $\tau(x)$ and different number of nodes N on each edge of the plate (Data: $b/a = 1, E_1 = 60.7 \text{ GPa}, G_{12} = 12 \text{ GPa}, \nu_{12} = 0.23, \nu_{21} = 0.094$).

Freq. No. n	Non-dimensional natural frequency $\Omega_n = a\sqrt{\frac{\omega^2 \rho h}{D_1}}$									[42]
	$N = 4$			$N = 8$			$N = 16$			
	$\tau = x$	$\tau = \sqrt{x}$	$\tau = x^2$	$\tau = x$	$\tau = \sqrt{x}$	$\tau = x^2$	$\tau = x$	$\tau = \sqrt{x}$	$\tau = x^2$	
1	1.5832	1.5832	1.5832	1.5832	1.5832	1.5832	1.5832	1.5832	1.5832	1.5832
2	1.8798	1.8793	1.8793	1.8795	1.8793	1.8793	1.8794	1.8793	1.8793	1.8793
3	2.3644	2.3653	2.3653	2.3657	2.3653	2.3653	2.3654	2.3653	2.3653	2.3653
4	2.4844	2.4843	2.4843	2.4863	2.4863	2.4863	2.4869	2.4875	2.4870	2.4872
5	2.7335	2.7335	2.7336	2.7345	2.7344	2.7345	2.7348	2.7349	2.7349	2.7349
6	3.1401	3.1401	3.1401	3.1394	3.1394	3.1393	3.1392	3.1394	3.1390	3.1388
7	3.4716	3.4892	3.4892	3.4851	3.4892	3.4892	3.4892	3.4892	3.4892	3.4892
8	3.5142	3.5142	3.5142	3.5142	3.5142	3.5142	3.5142	3.5142	3.5142	3.5142
9	3.9219	3.9220	3.9220	3.9214	3.9214	3.9214	3.9211	3.9214	3.9210	3.9210
10	4.1395	4.1395	4.1395	4.1395	4.1395	4.1395	4.1395	4.1395	4.1395	4.1395

Table 2

Convergence of results for a square orthotropic plate with CCCC boundary condition using the present method with different mesh distribution of nodes represented by $\tau(x)$ and different number of nodes N on each edge of the plate (Data: $b/a = 1, E_1 = 60.7 \text{ GPa}, G_{12} = 12 \text{ GPa}, \nu_{12} = 0.23, \nu_{21} = 0.094$).

Freq. No. n	Non-dimensional natural frequency $\Omega_n = a\sqrt{\frac{\omega^2 \rho h}{D_1}}$									[42]
	$N = 4$			$N = 8$			$N = 16$			
	$\tau = x$	$\tau = \sqrt{x}$	$\tau = x^2$	$\tau = x$	$\tau = \sqrt{x}$	$\tau = x^2$	$\tau = x$	$\tau = \sqrt{x}$	$\tau = x^2$	
1	2.6971	2.6975	2.6971	2.6974	2.6975	2.6974	2.6975	2.6975	2.6975	2.6975
2	3.5646	3.5645	3.5645	3.5649	3.5649	3.5649	3.5649	3.5649	3.5649	3.5649
3	4.1012	4.1012	4.1012	4.1014	4.1015	4.1014	4.1015	4.1015	4.1015	4.1015
4	4.6282	4.6283	4.6282	4.6283	4.6283	4.6283	4.6283	4.6283	4.6283	4.6283
5	4.6674	4.6678	4.6674	4.6677	4.6678	4.6678	4.6678	4.6678	4.6678	4.6678
6	5.4438	5.4438	5.4438	5.4446	5.4447	5.4447	5.4446	5.4446	5.4446	5.4446
7	5.6161	5.6157	5.6156	5.6156	5.6157	5.6157	5.6157	5.6157	5.6157	5.6157
8	5.8496	5.8496	5.8496	5.8497	5.8497	5.8497	5.8497	5.8497	5.8497	5.8497
9	5.9759	5.9759	5.9759	5.9759	5.9759	5.9759	5.9759	5.9759	5.9759	5.9759
10	6.4397	6.4397	6.4396	6.4397	6.4397	6.4397	6.4397	6.4397	6.4397	6.4397

Table 3

Convergence of results for a square orthotropic plate with CFCF boundary condition using the present method with different mesh distribution of nodes represented by $\tau(x)$ and different number of nodes N on each edge of the plate (Data: $b/a = 1, E_1 = 60.7 \text{ GPa}, G_{12} = 12 \text{ GPa}, \nu_{12} = 0.23, \nu_{21} = 0.094$).

Freq. No. n	Non-dimensional natural frequency $\Omega_n = a\sqrt{\frac{\omega^2 \rho h}{D_1}}$									[42]
	$N = 4$			$N = 8$			$N = 16$			
	$\tau = x$	$\tau = \sqrt{x}$	$\tau = x^2$	$\tau = x$	$\tau = \sqrt{x}$	$\tau = x^2$	$\tau = x$	$\tau = \sqrt{x}$	$\tau = x^2$	
1	2.3628	2.3624	2.3623	2.3628	2.3627	2.3627	2.3628	2.3628	2.3628	2.3628
2	2.4832	2.4832	2.4832	2.4847	2.4846	2.4846	2.4851	2.4851	2.4850	2.4849
3	2.9274	2.9316	2.9316	2.9302	2.9318	2.9318	2.9315	2.9318	2.9318	2.9318
4	3.7309	3.7309	3.7309	3.7412	3.7392	3.7392	3.7412	3.7411	3.7411	3.7412
5	3.9239	3.9239	3.9239	3.9235	3.9235	3.9235	3.9234	3.9235	3.9234	3.9233
6	4.0255	4.0255	4.0255	4.0255	4.0256	4.0255	4.0256	4.0256	4.0256	4.0256
7	4.3598	4.3598	4.3598	4.3558	4.3558	4.3558	4.3557	4.3558	4.3557	4.3557
8	4.7631	4.7793	4.7793	4.7770	4.7807	4.7807	4.7798	4.7807	4.7807	4.7807
9	4.9225	4.9225	4.9225	4.9244	4.9244	4.9244	4.9245	4.9245	4.9245	4.9245
10	5.4952	5.4941	5.4940	5.4945	5.4941	5.4941	5.4943	5.4941	5.4941	5.4941

Table 4

Comparison convergence of results for the CFFF square plate using the present theory and SEM [34] ($\nu = 0.3; a = 0.5 \text{ m}, h = 0.001 \text{ m}; E = 69 \text{ GPa}, \rho = 2700 \text{ kg/m}^3$).

Freq. No. n	Natural frequency $f_n = \frac{\omega_n}{2\pi}$ (Hz)							FEM [34] (ANSYS 200 × 200)
	SEM			Present theory				
	$N_{SEM} = 8$	$N_{SEM} = 32$	$N_{SEM} = 128$	$N = 8$	$N = 16$	$N = 32$		
1	0.843	0.845	0.845	0.844	0.845	0.845	0.845	
2	2.070	2.070	2.071	2.068	2.070	2.071	2.071	
3	5.177	5.180	5.182	5.180	5.181	5.182	5.182	
4	6.620	6.622	6.622	6.618	6.622	6.622	6.622	
5	7.532	7.534	7.536	7.533	7.536	7.536	7.537	

Table 5

The fundamental natural frequency Ω_1 for a square isotropic plate simply-supported on three edges and clamped along a length l symmetrically located in the middle on the third edge using the present theory with $N = 16$ and $\nu = 0.3$.

Fundamental natural frequency Ω_1									
$l/a = 0$		$l/a = 1/3$		$l/a = 1/2$		$l/a = 2/3$		$l/a = 1$	
Present theory	[4]	Present theory	[4]	Present theory	[4]	Present theory	[4]	Present theory	[4]
2.221	2.221	2.405	2.398	2.414	2.417	2.422	2.429	2.432	2.432

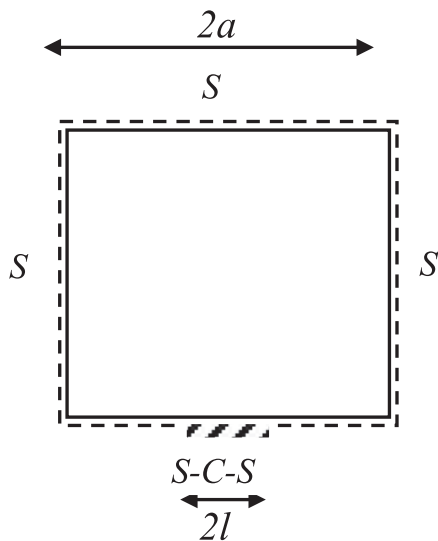


Fig. 3. A square plate simply-supported on the three edges and partial clamped support on the fourth edge along a length l symmetrically place in the middle.

centration at the center of the plate side. It should be noted that the use of an equally spaced mesh gives some distortion in the results for this example. Table 5 shows that if the l/a ratio is 0 or 1, i.e. if the side of the plate is simply-supported or fully clamped, the results from the current theory are exactly the same as those reported in [4,5]. When comparing results, it should be noted that in [4,5] the square of the non-dimensional frequency that has been defined in this paper was used. It may be explained that the results in [4,5] were obtained based on the method of Fourier series and in the limiting case, the results coincided with the exact solution of the problem obtainable from the Levy type of analysis. Clearly the current theory gives sufficiently accurate values of natural frequencies with $N = 16$. For other values of ratio l/a the results from the present theory are very close to those of [4,5].

The next example is an L-shaped isotropic plate which is symmetrical about the diagonal $x = y$ and the plate is clamped at all its edges, as shown in Fig. 4. For this problem comparative results are available in the literature [52]. The geometric and all other relevant data are taken from [52] in the current analysis. Note that the natural frequencies in non-dimensional form of isotropic clamped plates within the framework of Kirchoff-Love plate theory do not depend on any specific material constant or plate dimensions because of the non-dimensionalisation process, and understandably [52] gives the non-dimensional frequency parameter $\bar{\lambda}_n$ for the problem. Details of material properties, the thickness h and values of sides of the plate are absent in [52]. However, some of the parameters pertaining to Fig. 4 are given in [52]. These are: $a_1 = b_1$ and $a_2 = b_2 = 0.6a_1$. Table 6 shows the first five natural frequencies for the L-shaped plate using the proposed theory using $N = 16$ together with the results reported in [52] which are based on the method of double Fourier series. The natural frequencies computed using two very different theories, i.e., the proposed

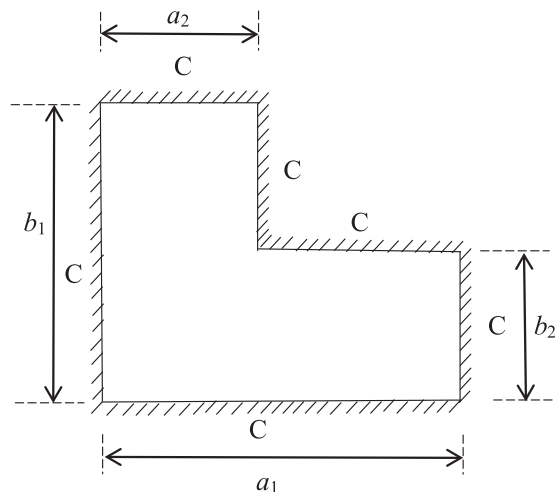


Fig. 4. An L shaped plate clamped at all edges [51].

Table 6

The first five non-dimensional natural frequencies $\bar{\lambda}_n = \frac{a_1}{\pi} \sqrt{\frac{h\rho\omega^2}{D}}$ ($n = 1, 2, \dots, 5$) of an L-shaped plate [51] with clamped edges $a_1:b_1:a_2:b_2 = 5:5:3:3$.

Freq. No n	Non-dimensional natural frequency $\bar{\lambda}_n$	
	Present theory with $N = 16$	Table 2 of Ref. [52]
1	2.409	2.40
2	2.914	2.91
3	3.265	3.26
4	3.867	3.86
5	3.911	3.90

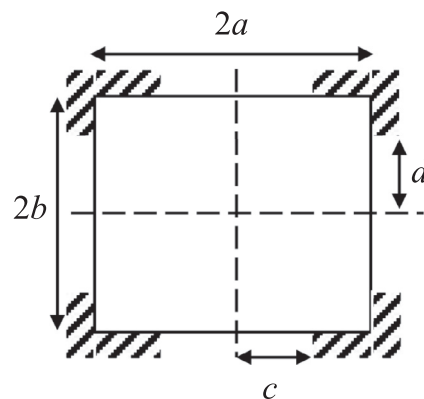


Fig. 5. A square plate clamped over a finite length at its corners.

theory and that of [52], see Table 2 of [52], are indeed extremely close. This is not surprising because both methods deal with exact solution of the governing differential equations, and as expected, both converge towards exact results. There might be some possible rounding errors in the results that are quoted in Table 2 from [52].

Table 7

The first ten non-dimensional natural frequencies Ω_n ($n = 1, 2, 3, \dots, 10$) for a square plate clamped over a finite length at its corners (Fig. 5) with $\nu = 0.3$, $E = 200$ GPa, $\rho = 7850$ kg/m³ and $c = 0.5a$ and $d = 0.75a$.

Freq. No n	Non-dimensional natural frequency $\Omega_n = a\sqrt{\frac{\omega^2 \rho h}{D}}$
1	1.5708
2	2.1878
3	2.2214
4	3.1415
5	3.5124
6	4.2082
7	4.3136
8	4.4428
9	4.4753
10	4.7123

The natural frequency parameters calculated with the help of the method of double Fourier series in [52] appears to have a slow convergence rate compared to the present method.

To further illustrate the usefulness of the proposed approach, two carefully chosen additional examples are now considered. The first one is a square isotropic plate clamped over a finite length

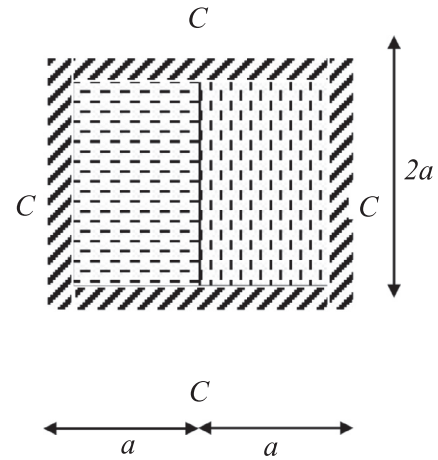


Fig. 7. Two orthotropic plates joined together and the assembly is clamped all-round the outer edges.

at the four corners of the plate as shown in Fig. 5. Corresponding to Fig. 5, the data used are: $a = 1$ m, $c = 0.5$ m and $d = 0.75$ m, $E = 200$ GPa, $\rho = 7850$ kg/m³ and $\nu = 0.3$. The solution for this type of prob-

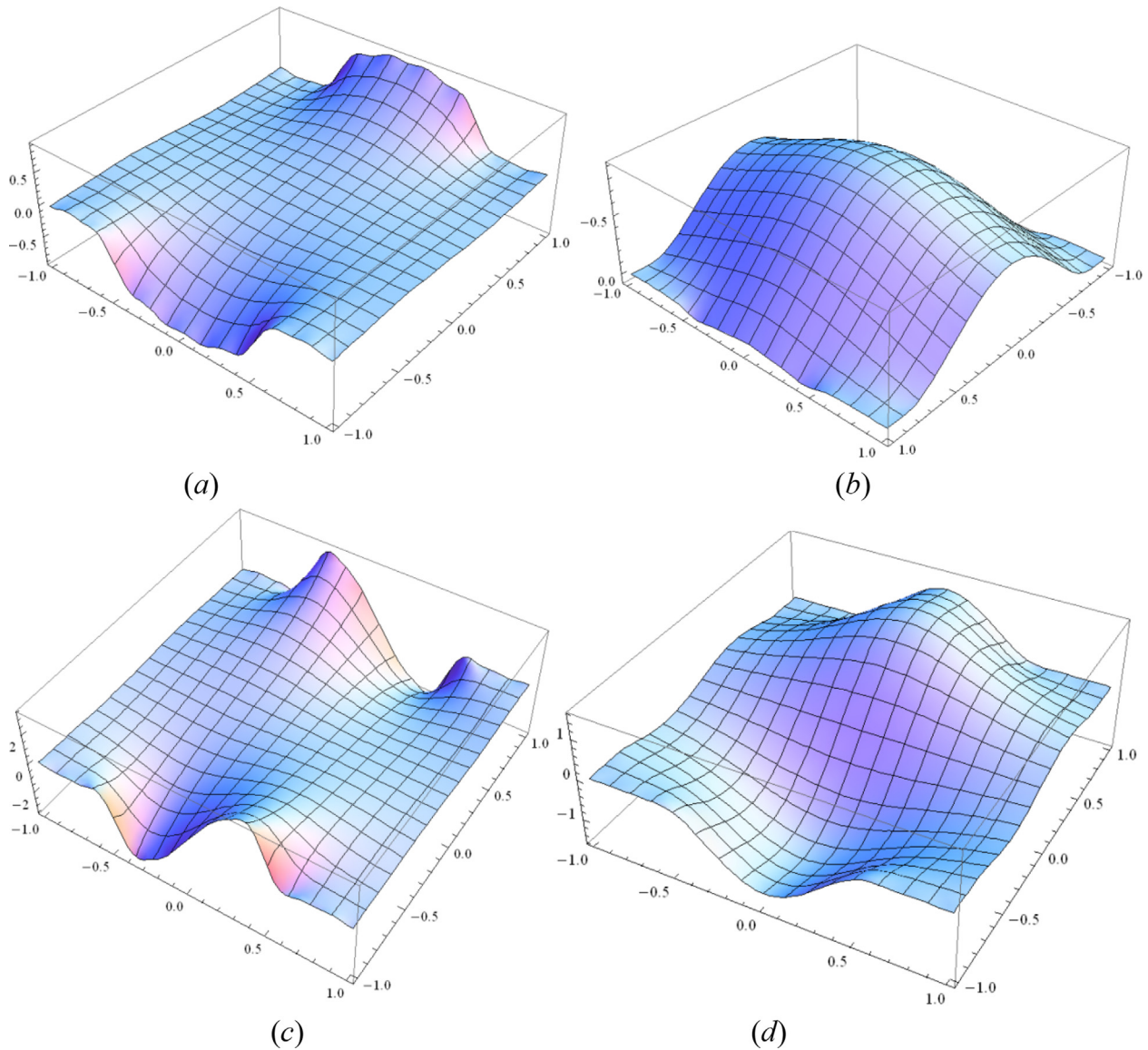


Fig. 6. The first (a), second (b), third (c) and fifth (d) natural modes of the plate in Fig. 5.

Table 8
The first ten natural frequencies Ω_n ($n = 1, 2, 3, \dots, 10$) of the plate shown in Fig. 7.

Freq. No n	Non-dimensional natural frequency $\Omega_n = a \sqrt{\frac{\rho^2 \beta h^3}{D_1}}$	Single quartz glass plate
		Assembly of two orthotropic plates (Fig. 7)
1	2.6823	2.6975
2	3.8172	3.5649
3	3.8367	4.1015
4	4.6408	4.6283
5	5.0246	4.6678
6	5.0389	5.4446
7	5.6394	5.6157
8	5.8515	5.8497
9	6.1962	5.9759
10	6.4692	6.4397

lem has not been reported in the literature and hence given for the first time. In the analysis 16 nodal points were chosen ($N = 16$) over the length ($a-c$) on the two corners of each of the top and bottom sides and the same number of nodes were chosen over the length ($b-d$) on two corners of each of the left-hand and right-hand sides of the plate. The node point distribution was chosen according to

the formula $\tau = \sqrt{x}$ (see Fig. 2) which gives node point concentration towards the end of the side. (It was noted that equally spaced node mesh with $\tau = x$ gave a weak convergence.) Table 7 gives the first ten natural frequencies of the plate in non-dimensional form whereas some selective mode shapes of the plate are shown in Fig. 6.

In the final example, two orthotropic composite plates are joined together, and the assembly of the two plates are clamped all-round the outer edges, see Fig. 7. The plate on the left has 0° ply orientation and the elastic constants are $E_1 = 60.7 \text{ GPa}, G_{12} = 12 \text{ GPa}, \nu_{12} = 0.23, \nu_{21} = 0.094$ whereas the plate on the right has 90° ply orientation so that the elastic constants are $E_2 = 60.7 \text{ GPa}, G_{12} = 12 \text{ GPa}, \nu_{12} = 0.094, \nu_{21} = 0.23$. Following the analysis, Table 8 shows the first ten natural frequencies of the composite plate shown in Fig. 7 together with those of a quartz glass plate with clamped edges (see Table 2). When computing the results of Table 8, the number of nodal points N was set to 16 and the distribution of nodes was based on the formula $\tau = \sqrt{x}$, see Fig. 2. The authors are surprised that most of the results shown in Table 8 show excellent agreement between the quartz plate and the composite plate of Fig. 7. The first, fourth and seventh, eighth and ninth natural frequencies show excellent

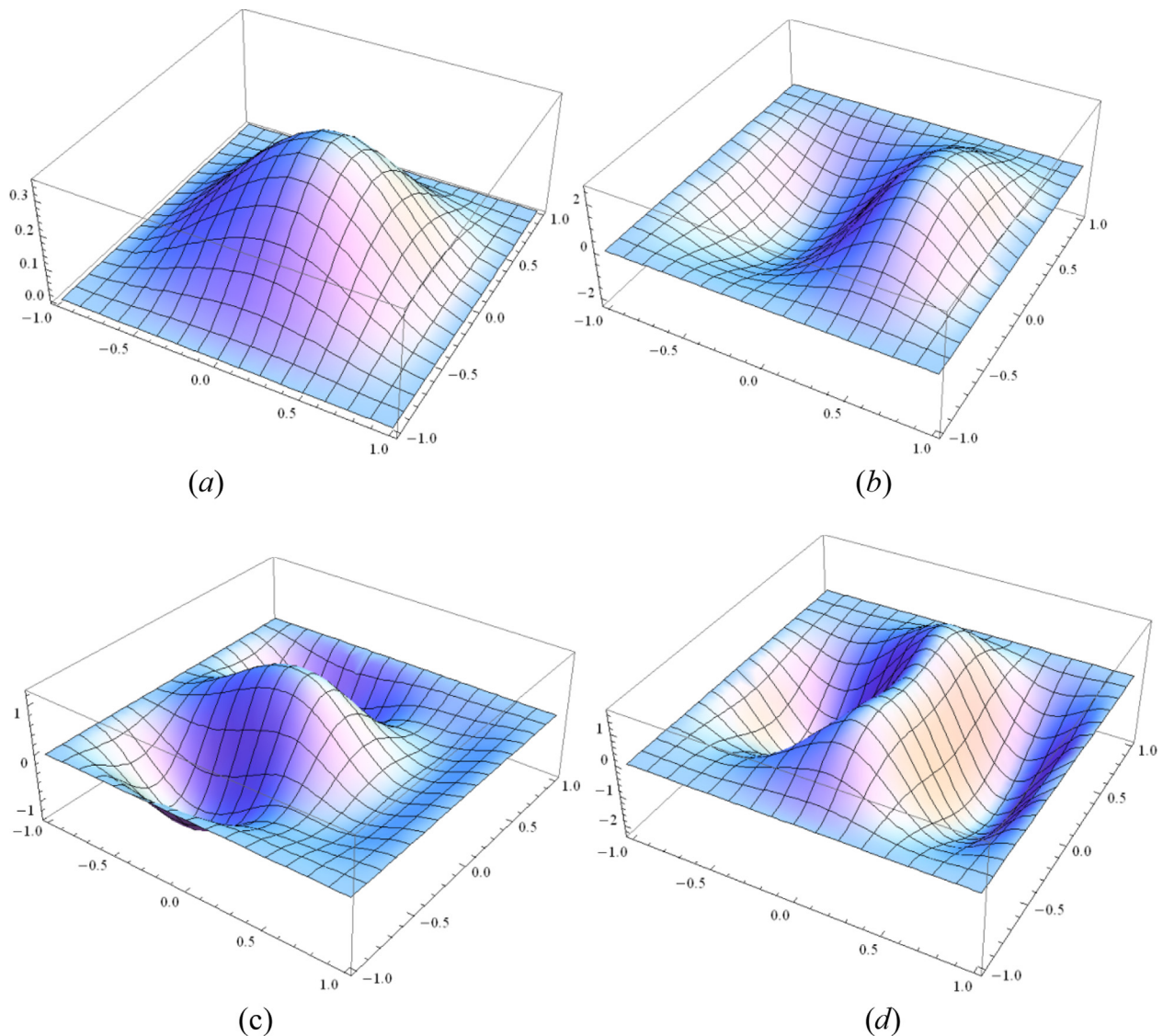


Fig. 8. The first (a), second (b), fifth (c) and sixth (d) mode shapes of the plate assembly shown in Fig. 7.

agreement with less than 1% discrepancy whereas the differences in the second, third, fifth and sixth natural frequencies are relatively larger, but they are all within 8%. Fig. 8 shows representative mode shapes for the two combined composite plate. It can be seen from Fig. 8 that the first and second mode shapes exhibit proper symmetry as expected from the single a square quartz glass plate with CCC edges, but there is significant asymmetry in the fifth and sixth mode shapes which is a consequence of composite nature of the plate shown in Fig. 7.

5. Conclusions

The principal novelty in this paper is the development of a new theory for the dynamic stiffness method for plates containing point nodes to carry out free vibration analysis of plates and plate assemblies. The amplitudes of the shear forces and bending moments at nodal points on the boundary of the plate are related to the corresponding amplitudes of the bending displacements and bending rotations through a system of linear equations to arrive at the ensuing dynamic stiffness matrix of the plate with point nodes. The formulation of dynamic stiffness matrix at nodal points of the plate has been possible by the application of the discrete Fourier transform for the modified system of trigonometric functions. The innovative discrete Fourier transform of this type applied in the context of this research has not been attempted before and is expected to pave the way for further research in the area. The analytical expressions for the direct and inverse Fourier transform for the case when the nodes are equally spaced are derived in an exact sense. The only approximation that arises is due to the point setting of the boundary condition because a point node formulation does not uniquely define a continuous function at the plate boundary, but as the authors have shown that the derived analytical solution satisfies exactly the governing differential equation for any set of nodal points. The theory is applied with particular reference to the Wittrick-Williams algorithm to compute the natural frequencies of a number of illustrative examples, but some results are checked by traditional approach of tracking the zeroes of the frequency determinant over a wide frequency range. The validity of the theory is confirmed by carefully selected sample of examples for which comparative results are available in the literature. Numerical examples show that a relatively small numbers of nodal points ($N = 8$ for continuous boundary conditions, and $N = 16$ for discontinuous boundary conditions) are adequate to determine the natural frequencies of isotropic and orthotropic plates and their assemblies with sufficient accuracy. The proposed method has the added advantage of setting the boundary conditions and/or assembling dissimilar elements directly at the nodal points. The results from the numerical simulations show that the use of non-uniform mesh of node distribution gives better accuracy than equally spaced arrangement of nodes.

Declaration of Competing Interest

The authors declare that they have no known competing financial interests or personal relationships that could have appeared to influence the work reported in this paper.

Acknowledgments

The authors acknowledge the help and support given by the Leverhulme Trust, UK (Grant Ref: EM-2019-061) and the Russian Science Foundation (Grant Ref: 22-21-00226, sections 3 and 4, <https://rscf.ru/project/22-21-00226>) which inspired this work.

Appendix A

Let a given function $f_k(x)$ is even (index $k = 0$) or odd (index $k = 1$) during the interval $[-a; a]$ and it is defined in $(N - 1 + k)$ equally spaced nodes at $x_n = a \frac{n}{N}$ where $n = k, k + 1, \dots, N$ and $f(x_n) = f_n$.

We define a discrete Fourier transform which maps the nodal values of the functions f and \tilde{f} defined below.

$$f = [f_k, f_{k+1}, \dots, f_N]^T \tag{A1}$$

$$\tilde{f} = [\tilde{f}_1, \tilde{f}_2, \dots, \tilde{f}_{N+1-k}]^T \tag{A2}$$

Following Eqs. (A1) and (A2), f_n and \tilde{f}_m can now be defined with respect to the following functions represented by a system of trigonometric functions $\{T_k(\alpha_{mn}x)\}$ so that.

$$f_n = \sum_{m=1}^{N+1-k} T_{nm} \tilde{f}_m \tag{A3}$$

$$\tilde{f}_m = \sum_{n=k}^N T_{mn}^{-1} f_n \tag{A4}$$

where $T_{nm} = T_k(\alpha_{mn}x_n)$ are elements of the matrix T for forward transform of dimension $(N - 1 + k)$.

For forward and inverse transform notation, Eqs. (A1) and (A2) can be written in matrix form as.

$$f = T \tilde{f} \tag{A5}$$

$$\tilde{f} = T^{-1} f \tag{A6}$$

It should be noted that it is not possible to explicitly construct the inverse matrix (inverse transform) T^{-1} using the values of the elements of the matrix T . This is because in contrast to the classical discrete Fourier transform, the conditions for the orthogonality of the basis functions at the nodal points are not satisfied in the presented case.

The trigonometric interpolation polynomial $f_N(x)$ is constructed in the following form.

$$f_N(x) = \sum_{m=1}^{N+1-k} \tilde{f}_m T_k(\alpha_{mk}x) \tag{A7}$$

In accordance with the standard technique of the method of least squares we minimize the function $R(\tilde{f})$ which is the square of the differences between $f_N(x_n)$ and f_n as expressed below.

$$\text{Minimize } R(\tilde{f}) = \sum_{n=k}^N (f_N(x_n) - f_n)^2 \tag{A8}$$

Then by using the condition of existence of stationary point of the function $R(\tilde{f})$, i.e., setting each of the first partial derivatives with respect to the each of the coefficients to zero to give

$$\frac{\partial R}{\partial \tilde{f}_m} = 0 \tag{A9}$$

In this way, one can derive the following system of linear algebraic equations (the so-called normal equations) for coefficients of the interpolation polynomial of Eq. (A7).

$$\sum_{m=1}^{N+1-k} M_{lm} \tilde{f}_m = \sum_{n=k}^N T_k(\alpha_{lk}x_n) f_n \quad (l = 1, 2, \dots, N + 1 - k) \tag{A10}$$

where

$$M_{lm} = \sum_{n=k}^N T_k(\alpha_{lk}x_n)T_l(\alpha_{mn}x_n) \tag{A11}$$

Now the system of Eq.(A10) can be rewritten in the following matrix form

$$M\tilde{f} = T^T f \tag{A12}$$

where T^T is transposed matrix T and

$$M = T^T T \tag{A13}$$

The matrix M depending upon the symmetry prescribed by the value of k of the considered functions system $\{T_k(\alpha_{mn}x)\}$ is established as follows. Thus, from the matrix relationship of Eq. (A12) we can determine the values of the Fourier coefficients \tilde{f} as follows

square is necessarily an interpolation polynomial. This type of general analysis is well known in the theory of classical discrete Fourier transform (see Bessel's formula [49]).

To prove the validity of the discrete Fourier transform, it is necessary to calculate the values of polynomial $f_N(x)$ at the nodal points, where they must coincide with the nodal values of the functions f . The following equalities prove this fact.

$$\begin{aligned} [f_N(x_k), f_N(x_{k+1}), \dots, f_N(x_N)]^T &= T\tilde{f} = TM^{-1}T^T f \\ &= T(T^T T)^{-1} T^T f \\ &= TT^{-1}(T^T)^{-1} T^T f = f \end{aligned} \tag{A16}$$

Based on Eq. (A16), it can be ascertained that Eqs. (A14) and (A15) are nothing but the inverse transform formulas for forward

If $k = 0$ and N is even number

$$M = \begin{pmatrix} N+1 & 0 & 1 & \dots & 0 & 1 \\ 0 & \frac{N}{2}+1 & 0 & \dots & 1 & 0 \\ 1 & 0 & \frac{N}{2}+1 & \dots & 0 & 1 \\ \dots & \dots & \dots & \dots & \dots & \dots \\ 0 & 1 & 0 & \dots & \frac{N}{2}+1 & 0 \\ 1 & 0 & 1 & \dots & 0 & N+1 \end{pmatrix}$$

If $k = 1$ and N is even number

$$M = \frac{1}{2} \begin{pmatrix} N+1 & -1 & 1 & \dots & 1 & -1 \\ -1 & N+1 & -1 & \dots & -1 & 1 \\ 1 & -1 & N+1 & \dots & 1 & -1 \\ \dots & \dots & \dots & \dots & \dots & \dots \\ 1 & -1 & 1 & \dots & N+1 & -1 \\ -1 & 1 & -1 & \dots & -1 & N+1 \end{pmatrix}$$

If $k = 0$ and N is odd number

$$M = \begin{pmatrix} N+1 & 0 & 1 & \dots & 1 & 0 \\ 0 & \frac{N}{2}+1 & 0 & \dots & 0 & 1 \\ 1 & 0 & \frac{N}{2}+1 & \dots & 1 & 0 \\ \dots & \dots & \dots & \dots & \dots & \dots \\ 1 & 0 & 1 & \dots & \frac{N}{2}+1 & 0 \\ 0 & 1 & 0 & \dots & 0 & N+1 \end{pmatrix}$$

If $k = 1$ and N is odd number

$$M = \frac{1}{2} \begin{pmatrix} N+1 & -1 & 1 & \dots & -1 & 1 \\ -1 & N+1 & -1 & \dots & 1 & -1 \\ 1 & -1 & N+1 & \dots & -1 & 1 \\ \dots & \dots & \dots & \dots & \dots & \dots \\ -1 & 1 & -1 & \dots & N+1 & -1 \\ 1 & -1 & 1 & \dots & -1 & N+1 \end{pmatrix}$$

$$\tilde{f} = M^{-1}T^T f \tag{A14}$$

Equation (A14) in expanded form can be rewritten as.

$$\tilde{f}_m = \sum_{n=k}^N \left\{ \sum_{l=1}^{N+1-k} \sigma_{ml} T_l(\alpha_{lk}x_n) \right\} f_n \tag{A15}$$

where σ_{ml} are the elements of the matrix $\sigma = M^{-1}$.

If the coefficients of trigonometric polynomial of Eq. (A7) are calculated according to the Eq. (A14) and (A15) then its values at the nodal points coincide with the given values of function $f(x)$, i.e. $f_N(x_n) = f_n$. Thus, the polynomial $f_N(x)$ obtained by minimizing the difference in Eq. (A8) with the help of the method of least

Fourier transform of the expressions given by Eqs. (A4) and (A6). In this case, the inverse transformation matrix can be calculated from.

$$T^{-1} = \sigma T^T \tag{A17}$$

Given below are the explicit expressions for the matrix $\sigma = M^{-1}$ for different values of k which signifies the type of symmetry. For the equally spaced nodes the inverse matrix $\sigma = M^{-1}$ always exists. It follows that the sequences of real numbers f and \tilde{f} are a pair of discrete Fourier transform.

if $k = 0$ and N is even number

$$\sigma = \frac{1}{N^2} \begin{pmatrix} N-\frac{1}{2} & 0 & -1 & 0 & -1 & \dots & -1 & 0 & -\frac{1}{2} \\ 0 & 2N-2 & 0 & -2 & 0 & \dots & 0 & -2 & 0 \\ -1 & 0 & 2N-2 & 0 & -2 & \dots & -2 & 0 & -1 \\ 0 & -2 & 0 & 2N-2 & 0 & \dots & 0 & -2 & 0 \\ -1 & 0 & -2 & 0 & 2N-2 & \dots & -2 & 0 & -1 \\ \dots & \dots \\ -1 & 0 & -2 & 0 & -2 & \dots & 2N-2 & 0 & -1 \\ 0 & -2 & 0 & -2 & 0 & \dots & 0 & 2N-2 & 0 \\ -\frac{1}{2} & 0 & -1 & 0 & -1 & \dots & -1 & 0 & N-\frac{1}{2} \end{pmatrix}$$

if $k = 1$ and N is even number

$$\sigma = \frac{1}{N^2} \begin{pmatrix} 2N-1 & 1 & -1 & \dots & -1 & 1 \\ 1 & 2N-1 & 1 & \dots & 1 & -1 \\ -1 & 1 & 2N-1 & \dots & -1 & 1 \\ \dots & \dots & \dots & \dots & \dots & \dots \\ -1 & 1 & -1 & \dots & 2N-1 & 1 \\ 1 & -1 & 1 & \dots & 1 & 2N-1 \end{pmatrix}$$

if $k = 0$ and N is odd number

$$\sigma = \frac{1}{N^2} \begin{pmatrix} N-\frac{1}{2} & 0 & -1 & 0 & -1 & \dots & 0 & -1 & 0 \\ 0 & 2N-2 & 0 & -2 & 0 & \dots & -2 & 0 & -1 \\ -1 & 0 & 2N-2 & 0 & -2 & \dots & 0 & -2 & 0 \\ 0 & -2 & 0 & 2N-2 & 0 & \dots & -2 & 0 & -1 \\ -1 & 0 & -2 & 0 & 2N-2 & \dots & 0 & -2 & 0 \\ \dots & \dots \\ 0 & -2 & 0 & -2 & 0 & \dots & 2N-2 & 0 & -1 \\ -1 & 0 & -2 & 0 & -2 & \dots & 0 & 2N-2 & 0 \\ 0 & -1 & 0 & -1 & 0 & \dots & -1 & 0 & N-\frac{1}{2} \end{pmatrix}$$

if $k = 1$ and N is odd number

$$\sigma = \frac{1}{N^2} \begin{pmatrix} 2N-1 & 1 & -1 & \dots & 1 & -1 \\ 1 & 2N-1 & 1 & \dots & -1 & 1 \\ -1 & 1 & 2N-1 & \dots & 1 & -1 \\ \dots & \dots & \dots & \dots & \dots & \dots \\ 1 & -1 & 1 & \dots & 2N-1 & 1 \\ -1 & 1 & -1 & \dots & 1 & 2N-1 \end{pmatrix}$$

References

- [1] Wittrick WH, Williams FW. Buckling and vibration of anisotropic or isotropic plate assemblies under combined loadings. *Int J Mech Sci* 1974;16(4):209–39. [https://doi.org/10.1016/0020-7403\(74\)90069-1](https://doi.org/10.1016/0020-7403(74)90069-1).
- [2] Wittrick WH, Williams FW. A general algorithm for computing natural frequencies of elastic structures. *Quart J Mech Appl Math* 1970;24(3):263–84. <https://doi.org/10.1093/qjmath/24.3.263>.
- [3] Wittrick WH, Williams FW. An algorithm for computing critical buckling loads of elastic structures. *J Struct Mech* 1973;1(4):497–518. <https://doi.org/10.1080/03601217308905354>.
- [4] Leissa AW. Vibration of plates. NASA Technical Report. NASA SP-160 1969. <https://doi.org/10.1002/zamm.19710510331>.
- [5] Leissa AW. The free vibration of rectangular plates. *J Sound Vib* 1973;31(1):257–93. [https://doi.org/10.1016/S0022-460X\(73](https://doi.org/10.1016/S0022-460X(73)
- [6] Prakash BG. Free vibration of rectangular plates. *J Sound Vib* 1980;70(2):303–5. [https://doi.org/10.1016/0022-460X\(80\)90602-1](https://doi.org/10.1016/0022-460X(80)90602-1).
- [7] Ramu I, Mohanty SC. Study on free vibration analysis of rectangular plate structures using finite element method. *Procedia Eng* 2012;38:2758–66. <https://doi.org/10.1016/j.proeng.2012.06.323>.
- [8] Yadav DPS, Sharma AK, Shivhare V. Free vibration analysis of isotropic plate with stiffeners using finite element method. *Eng Solid Mech* 2015;3:167–76. <https://doi.org/10.5267/j.esm.2015.5.002>.
- [9] Whitney JM. Free Vibration of Anisotropic Rectangular Plates. *J Acous Soc Amer* 1972;52:448–9. <https://doi.org/10.1121/1.1913115>.
- [10] Shufrin I, Eisenberger M. Stability and vibration of shear deformable plates—first order and higher order analyses. *Int J Solids Struct* 2005;42(3–4):1225–51. <https://doi.org/10.1016/j.ijsolstr.2004.06.067>.
- [11] Brischetto S, Carrera E. Importance of higher order modes and refined theories in free vibration analysis of composite plates. *J Appl Mech* 2010;77(011013–1):011013–4. <https://doi.org/10.1115/1.3173605>.
- [12] Mukhtar FM. Free vibration analysis of orthotropic plates by differential transform and Taylor collocation methods based on a refined plate theory. *Arch Appl Mech* 2017;87(1):15–40. <https://doi.org/10.1007/s00419-016-1172-2>.
- [13] Bhat RB. Natural frequencies of rectangular plates using characteristic orthogonal polynomials in Rayleigh-Ritz method. *J Sound Vib* 1985;102(4):493–9. [https://doi.org/10.1016/S0022-460X\(85\)80109-7](https://doi.org/10.1016/S0022-460X(85)80109-7).
- [14] Dawe DJ, Roufaeil OL. Rayleigh-Ritz vibration analysis of Mindlin plates. *J sound Vib* 1980;69(3):345–59. [https://doi.org/10.1016/0022-460X\(80\)90477-0](https://doi.org/10.1016/0022-460X(80)90477-0).
- [15] Liew KM, Wang CM. Vibration analysis of plates by the pb-2 rayleigh-Ritz method: mixed boundary conditions, reentrant corners, and internal curved supports. *Mech Struct Machines* 1992;20(3):281–92. <https://doi.org/10.1080/08905459208905170>.
- [16] Singhatanadgip P, Taranajetsada P. Vibration analysis of stepped rectangular plates using the extended Kantorovich method. *Mech Adv Mater Struct* 2016;23(2):201–15. <https://doi.org/10.1080/15376494.2014.949922>.
- [17] Ng SF, Y. Aaraa Y. Free vibration and buckling analysis of clamped rectangular plates of variable thickness by the Galerkin method. *J Sound Vib* 1989;135(2):263–274. [https://doi.org/10.1016/0022-460X\(89\)90725-6](https://doi.org/10.1016/0022-460X(89)90725-6).
- [18] Gorman DJ. Free vibration analysis of completely free rectangular plates by the superposition-Galerkin method. *J Sound Vib* 2000;237(5):901–14. <https://doi.org/10.1006/jsvi.2000.3151>.
- [19] Bert CW, Xinwei W, Striz AG. Differential quadrature for static and free vibration analyses of anisotropic plates. *Int J Solids Struct* 1993;30(13):1737–44. [https://doi.org/10.1016/0020-7683\(93\)90230-5](https://doi.org/10.1016/0020-7683(93)90230-5).
- [20] Katsikadelis JT. A boundary element solution to the vibration problem of plates. *J Sound Vib* 1990;141(2):313–22. [https://doi.org/10.1016/0022-460X\(90\)90842-N](https://doi.org/10.1016/0022-460X(90)90842-N).
- [21] Pereira WLA, Karam VJ, Carrer JAM, Mansur WJ. A dynamic formulation for the analysis of thick elastic plates by the boundary element method. *Eng Anal Bound Elem* 2012;36(7):1138–50. <https://doi.org/10.1016/jenganabound.2012.02.002>.
- [22] Boscolo M, Banerjee JR. Dynamic stiffness elements and their applications for plates using first order shear deformation theory. *Comput Struct* 2011;89:395–410. <https://doi.org/10.1016/j.compstruc.2010.11.005>.
- [23] Boscolo M, Banerjee JR. Dynamic stiffness formulation for composite Mindlin plates for exact modal analysis of structures. Part I: theory *Comput Struct* 2012;96–97:61–73. <https://doi.org/10.1016/j.compstruc.2012.01.002>.
- [24] Pagani A, Boscolo M, Banerjee JR, Carrera E. Exact dynamic stiffness elements based on one-dimensional higher-order theories for free vibration analysis of solid and thin-walled structures. *J Sound Vib* 2013;332:6104–27. <https://doi.org/10.1016/j.jsv.2013.06.023>.
- [25] Eisenberger M, Deutsch A. Solution of thin rectangular plate vibrations for all combinations of boundary conditions. *J Sound Vib* 2019;452:1–12. <https://doi.org/10.1016/j.jsv.2019.03.024>.
- [26] Casimir JB, Kevorkian S, Vinh T. The dynamic stiffness matrix of two-dimensional elements: application to Kirchhoff's plate continuous elements. *J Sound Vib* 2005;287(3):571–89. <https://doi.org/10.1016/j.jsv.2004.11.013>.
- [27] Ghorbel O, Casimir JB, Hammami L, Tawfiq I, Haddar M. Dynamic stiffness formulation for free orthotropic plates. *J Sound Vib* 2015;346:361–75. <https://doi.org/10.1016/j.jsv.2015.02.020>.
- [28] Fazzolari FA. A refined dynamic stiffness element for free vibration analysis of cross-ply laminated composite cylindrical and spherical shallow shells. *J Sound Vib* 2014;62:143–58. <https://doi.org/10.1016/j.compositesb.2014.02.021>.
- [29] Chen X, Ye K. Comparison Study on the Exact Dynamic Stiffness Method for Free Vibration of Thin and Moderately Thick Circular Cylindrical Shells. *Shock Vib* 2016; Article ID 9748135, 14 pages. <https://doi.org/10.1155/2016/9748135>.
- [30] Anderson MS, Williams FW, Banerjee JR, Durling BJ, Herstorm CL, Kennedy D, et al. User manual for BUNVIS-RG: An exact buckling and vibration program for lattice structures, with repetitive geometry and substructuring options. NASA Technical Memorandum 1986;87669. <https://doi.org/10.2514/6.1986-868>.
- [31] Williams FW, Kennedy D, Butler R. VICONOPT: Program for exact vibration and buckling analysis of analysis or design of prismatic plate assemblies. *AIAA J* 1991;29(11):1927–8. <https://doi.org/10.2514/3.10820>.
- [32] Nefovska-Danilovich M, Petronijevic M. In-plane free vibration and response analysis of isotropic rectangular plates using the dynamic stiffness method. *Comput Struct* 2015;152:82–95. <https://doi.org/10.1016/j.compstruc.2015.02.001>.
- [33] Nefovska-Danilovich M, Kolarevich N, Marjanovich M, Petronijevic M. Shear deformable dynamic stiffness elements for a free vibration analysis of composite plate assemblies – Part I: Theory. *Compos Struct* 2017;159:728–44. <https://doi.org/10.1016/j.compstruc.2016.09.022>.
- [34] Kim T, Lee U. Exact frequency-domain spectral element model for the transverse vibration of a rectangular Kirchhoff plate. *J Sound Vib* 2021;492:.. <https://doi.org/10.1016/j.jsv.2020.11.5812115812>.
- [35] Gorman DJ. Free vibration analysis of the completely free rectangular plate by the method of superposition. *J Sound Vib* 1978;57(3):437–47. [https://doi.org/10.1016/0022-460X\(78\)90322-X](https://doi.org/10.1016/0022-460X(78)90322-X).
- [36] Gorman DJ, Yu SD. A review of the superposition method for computing free vibration eigenvalues of elastic structures. *Comput Struct* 2012;104–105:27–37. <https://doi.org/10.1016/j.compstruc.2012.02.018>.
- [37] Gorman DJ. Free vibration analysis of rectangular plates. New-York: Elsevier, North Holland; 1982. <https://doi.org/10.1121/1.388465>.
- [38] Banerjee JR, Papkov SO, Liu X, Kennedy D. Dynamic stiffness matrix of a rectangular plate for the general case. *J Sound Vib* 2015;342:177–99. <https://doi.org/10.1016/j.jsv.2014.12.031>.
- [39] Papkov SO. Asymptotically Exact Solution of the Problem of Harmonic Vibrations of an Elastic Parallelepiped. *Mech Solids* 2017;52:686–99. <https://doi.org/10.3103/S0025654417060085>.
- [40] Liu X, Banerjee JR. An exact spectral-dynamic stiffness method for free flexural vibration analysis of orthotropic composite plate assemblies. Part I: Theory *Comput Struct* 2015;132:1274–87. <https://doi.org/10.1016/j.compstruc.2015.07.020>.
- [41] Wei Z, Yin X, Yu S, Wu W. Dynamic stiffness formulation for transverse and in-plane vibration of rectangular plates with arbitrary boundary conditions based on a generalized superposition method. *Int J Mech Mater Des* 2020. <https://doi.org/10.1007/s10999-020-09515-9>.
- [42] Papkov SO, Banerjee JR. Dynamic stiffness formulation and free vibration analysis of specially orthotropic Mindlin plates with arbitrary boundary conditions. *J Sound Vib* 2019;458:522–43. <https://doi.org/10.1016/j.jsv.2019.06.028>.
- [43] Papkov SO, Banerjee JR. A new method for free vibration and buckling analysis of rectangular orthotropic plates. *J Sound Vib* 2015;339:342–58. <https://doi.org/10.1016/j.jsv.2014.11.007>.
- [44] Kulla PH. High precision finite elements. *Finite Elem Anal Des* 1997;26(26):97–114. [https://doi.org/10.1016/S0168-874X\(96\)00073-X](https://doi.org/10.1016/S0168-874X(96)00073-X).
- [45] Doyle JF. *Wave Propagation in Structures: An FFT-Based Spectral Analysis Methodology*. Springer-Verlag; 1989.
- [46] Lee U. *The spectral element method in structural dynamics*. John Wiley; 2009. ISBN: 978-0-470-82375-0.
- [47] Birgersson F, Finnveden S, Nilsson C-M. A spectral super element for modelling of plate vibration. Part 1: general theory. *J Sound Vib* 2005;287:297–314. <https://doi.org/10.1016/j.jsv.2004.11.012>.
- [48] Hashemi SM. The use of trigonometric interpolation functions for vibration analysis of beam structures-bridging gap between FEM and exact formulation. *WIT Press*; 2004. p. 71. ISSN 1743–3509.
- [49] Prudnikov AP, Brychkov YA, Marichev OI. *Integrals and Series: Elementary Functions*. CRC Press; 1998.
- [50] Bracewell RN. *The Fourier transform and its applications*. New York: McGraw Hill; 2000.
- [51] Wolberg J. *Data Analysis Using the Method of Least Squares*. Berlin, Heidelberg: Springer; 2006.
- [52] Irie T, Yamada G, Narita Y. Free vibration of cross-shaped, I-shaped and L-shaped plates clamped at all edges. *J Sound Vib* 1978;61(4):571–83. [https://doi.org/10.1016/0022-460X\(78\)90456-X](https://doi.org/10.1016/0022-460X(78)90456-X).